SUPPORTING INFORMATION

Enhanced Rates of C-H Bond Cleavage by a Hydrogen Bonded Synthetic Heme High-Valent Iron(IV) Oxo Complex

Melanie A. Ehudin,[†] David A. Quist,[†] Kenneth D. Karlin*,[†]

[†] Department of Chemistry, Johns Hopkins University, Baltimore, Maryland 21218, United States

Table of Contents:

I. ^{1}H NMR spectra of xanthene-d_2 and 9,10-dihydroanthracene-d_4.

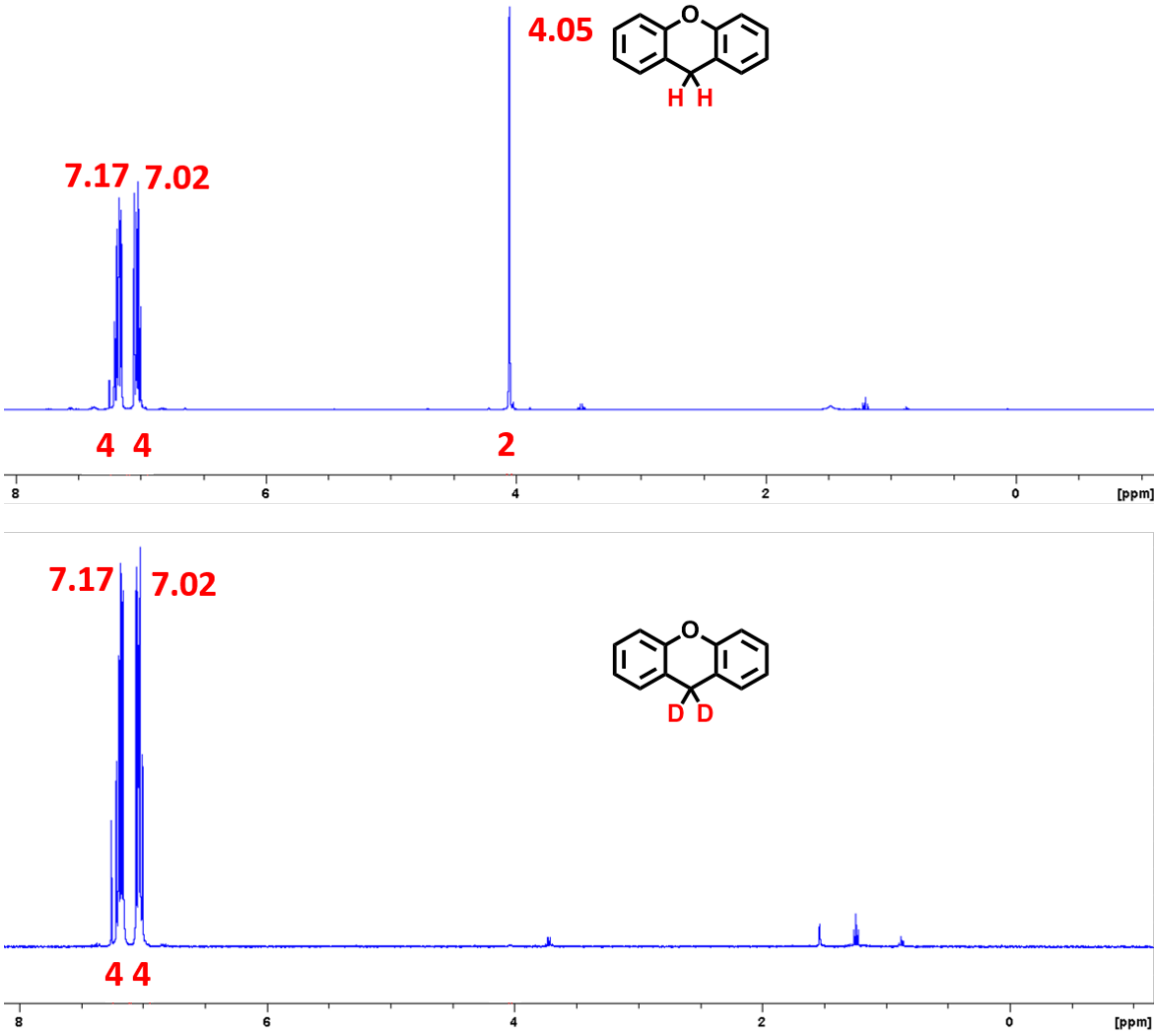

Figure S1. ^{1}H-NMR ($CDCl_3$, 400 MHz) spectra of xanthene (**top**) and xanthene-d_2 (**bottom**). Note that the resonance peak typically at 4.05 ppm of xanthene is of diminished intensity for xanthene-d_2.

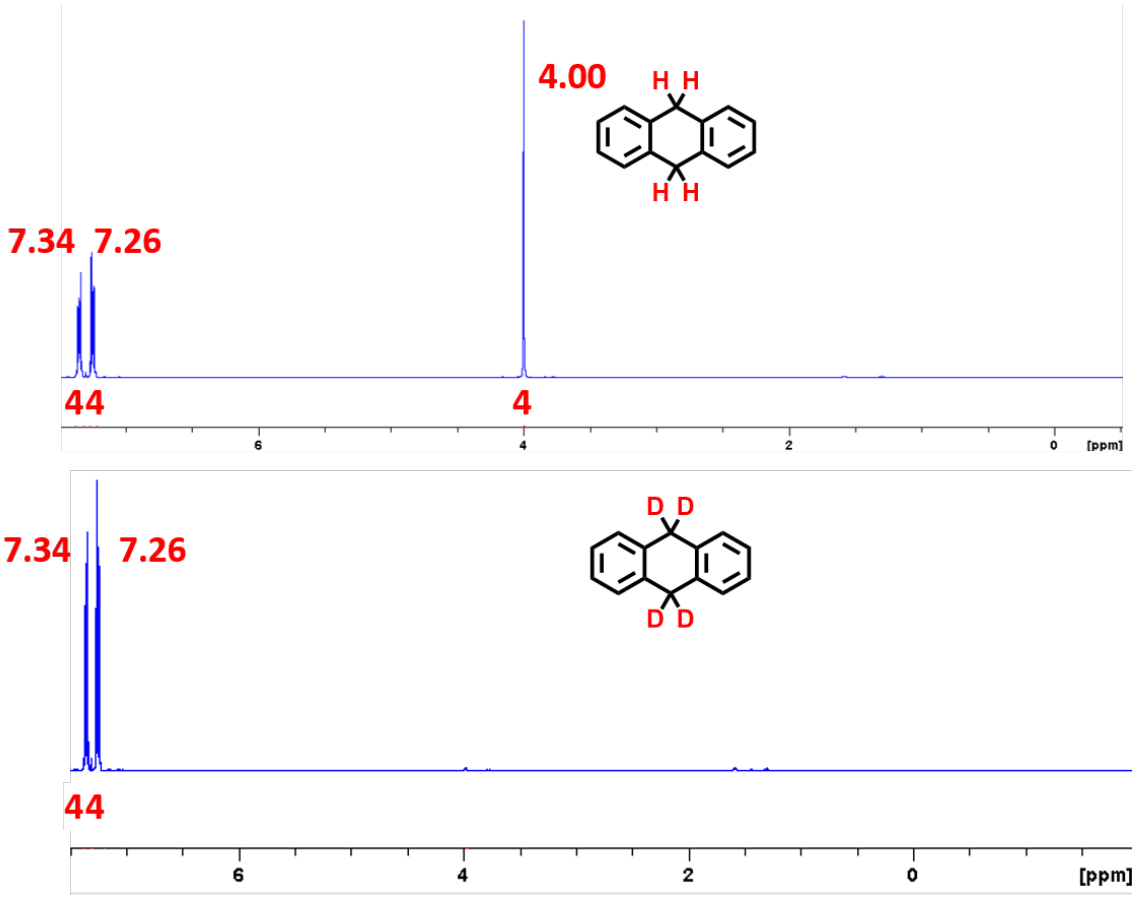

Figure S2. ^{1}H-NMR ($CDCl_3$, 400 MHz) spectra of 9,10-dihydroanthracene (**top**) and 9,10-dihydroanthracene-d_4 (**bottom**). Note that the resonance peak typically at 4.00 ppm of DHA is of diminished intensity for DHA-d_4.

II. UV-vis and EPR spectroscopy monitoring the reactivity between various C–H or C–D substrates and F_8Cmpd-II or F_8Cmpd-II(LutH$^+$). The resulting ferric product was quantified by EPR spectroscopy.

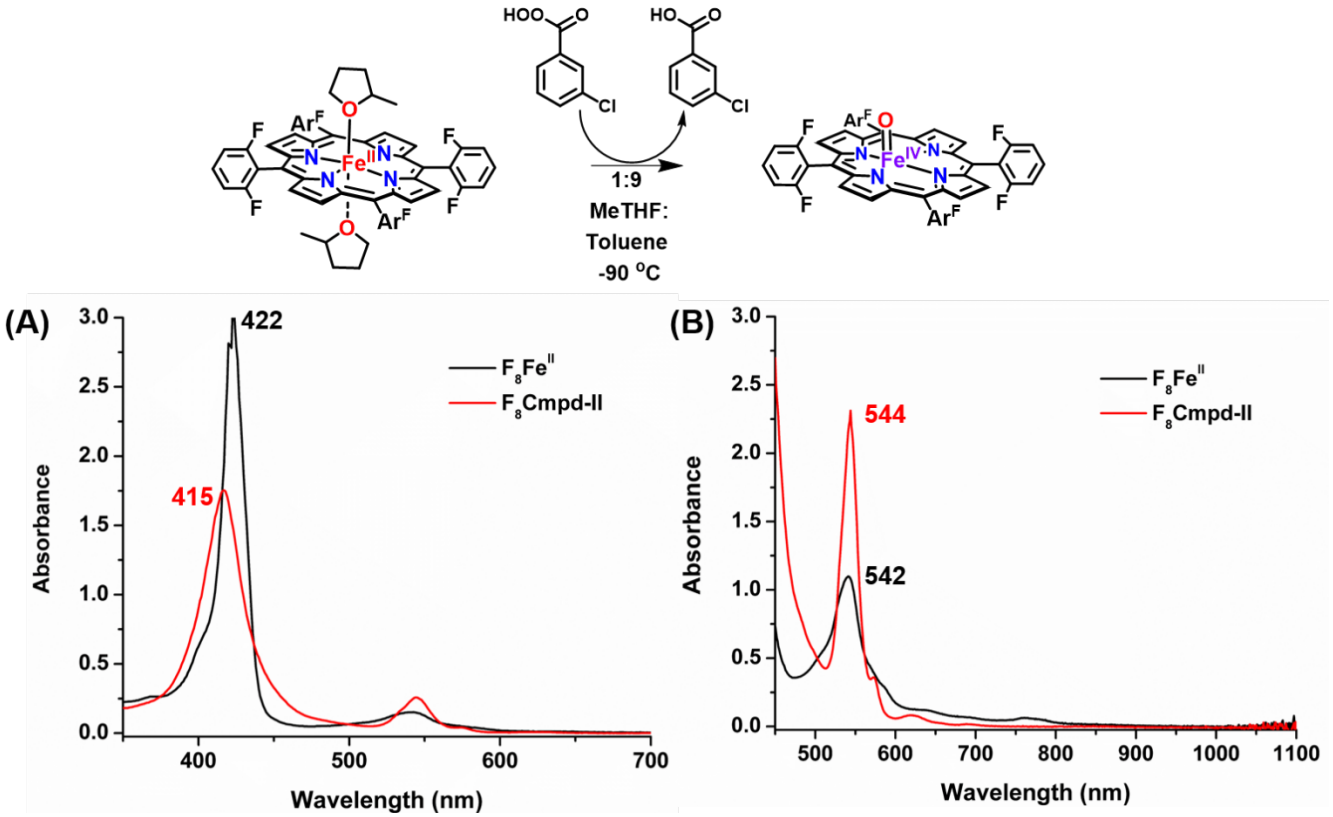

Figure S3. UV-vis monitoring of the addition of 1 equiv. *meta*-chloroperoxybenzoic acid (*m*CPBA) to F_8Fe^{II} at 0.01 mM (**A**) and 0.1 mM (**B**) at -90 °C in 1:9 MeTHF:toluene, resulting in the formation of the F_8Cmpd-II (**black** to **red**).

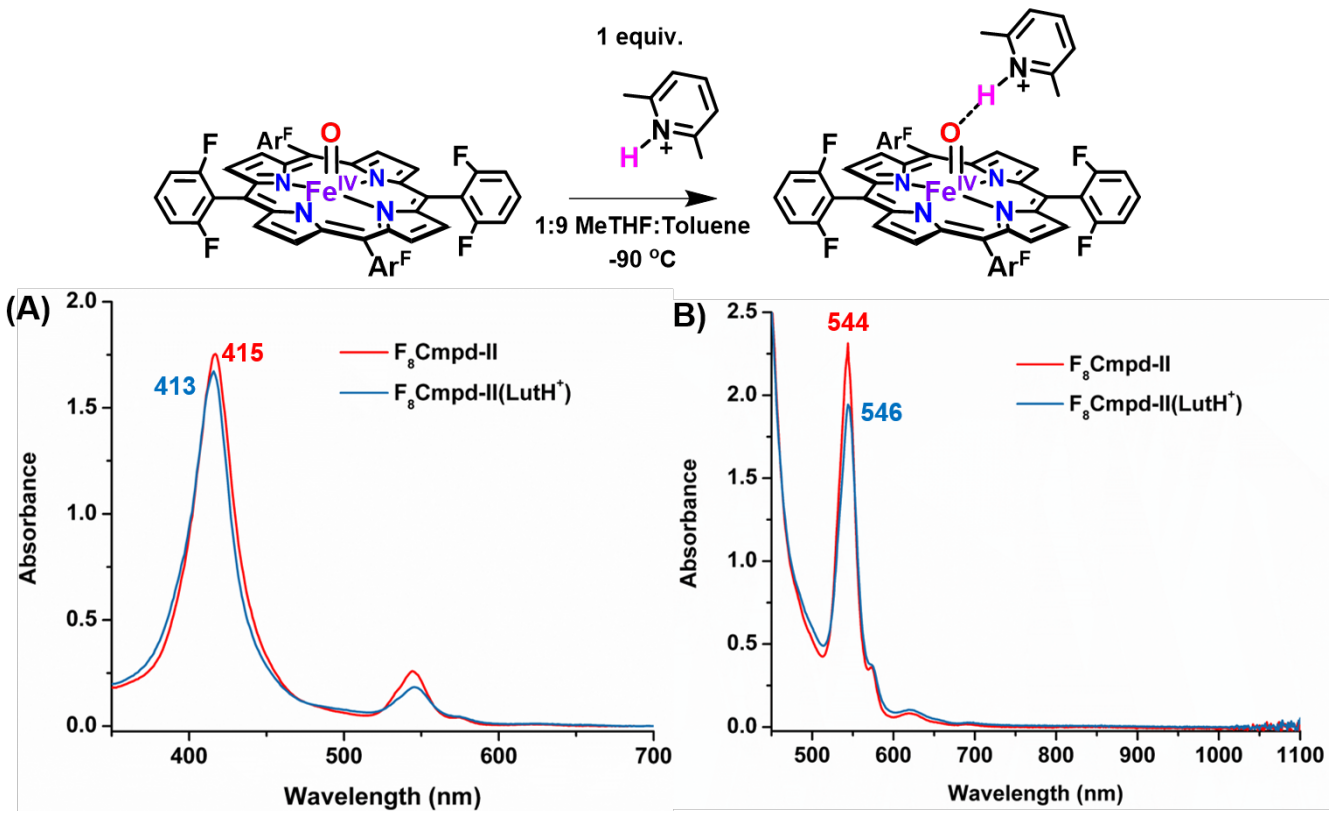

Figure S4. UV-vis monitoring of the addition of 1 equiv. 2,6-lutidinium triflate ($LutH^+$) to F_8Cmpd-II at 0.01 mM (**A**) and 0.1 mM (**B**) at -90 °C in 1:9 MeTHF:toluene, resulting in the formation of the F_8Cmpd-II($LutH^+$) (**red** to **blue**).

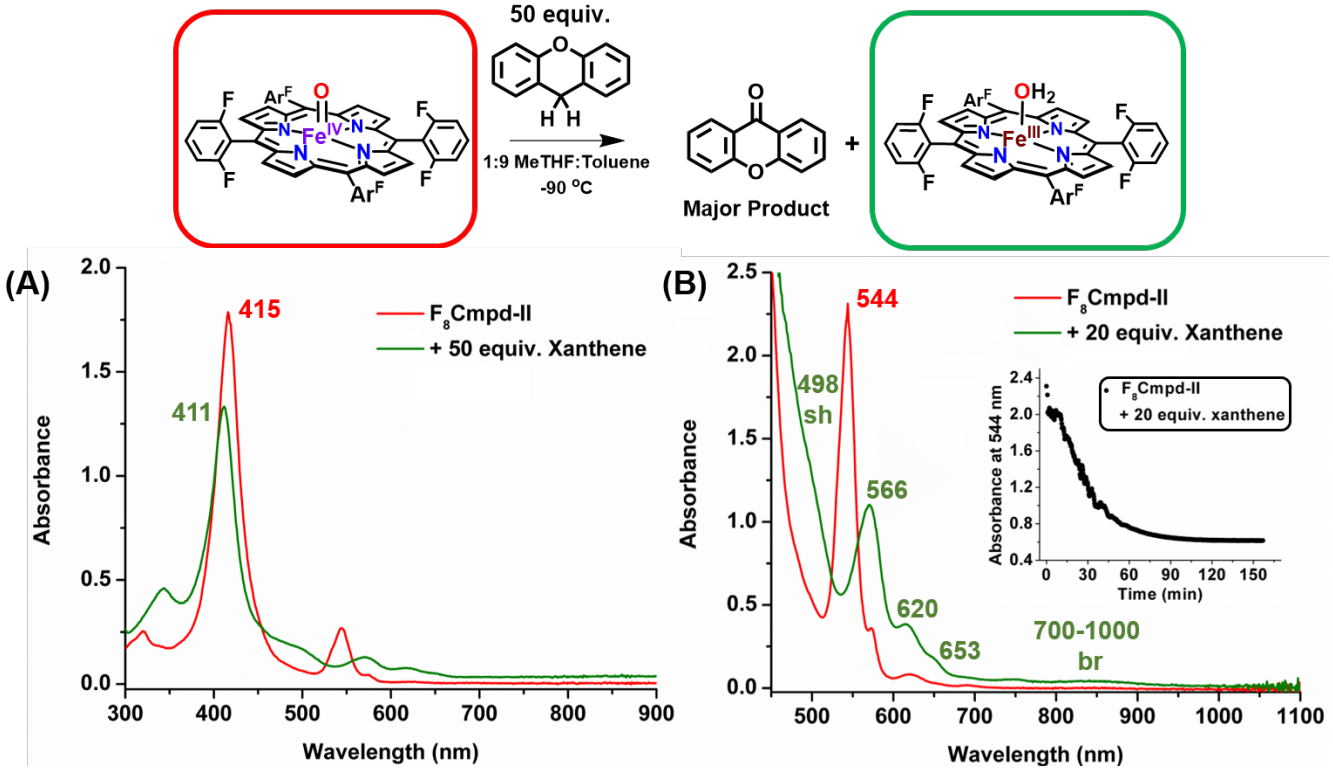

Figure S5. UV-vis monitoring of the addition of xanthene to F_8Cmpd-II at 0.01 mM (**A**) and 0.1 mM (**B**) at -90 °C in 1:9 MeTHF:toluene, resulting in the formation of the ferric aqua species (**red** to **green**). Inset: Decrease in the absorbance at 544 nm over time.

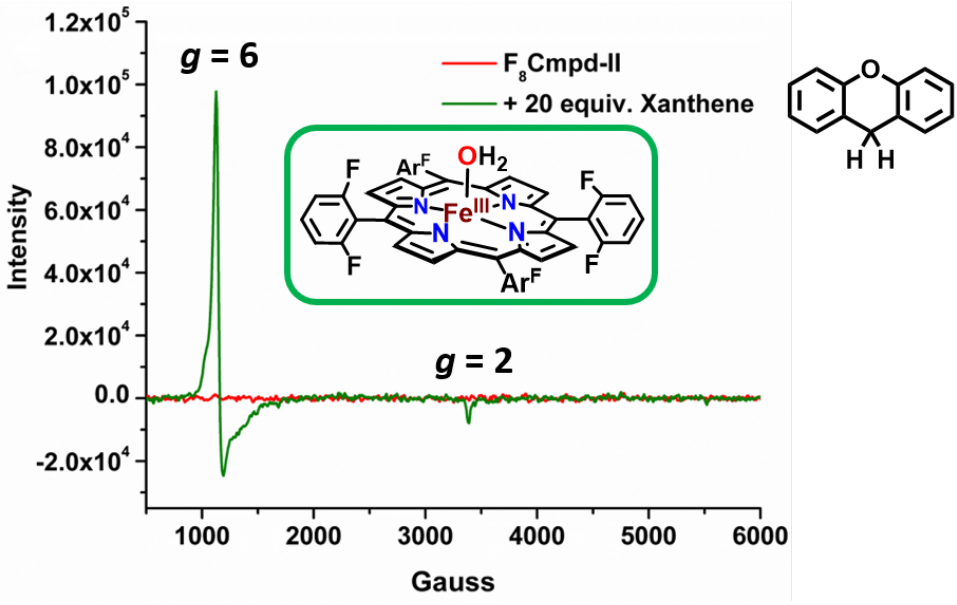

Figure S6. EPR spectra following the addition of 20 equiv. xanthene to F_8Cmpd-II at 2 mM in 1:9 MeTHF:toluene at -90 °C , resulting in the formation of the ferric aqua species (**red** to **green**).

The reaction was allowed to react for an hour before freezing the solution and acquiring an EPR spectrum at 10 K.

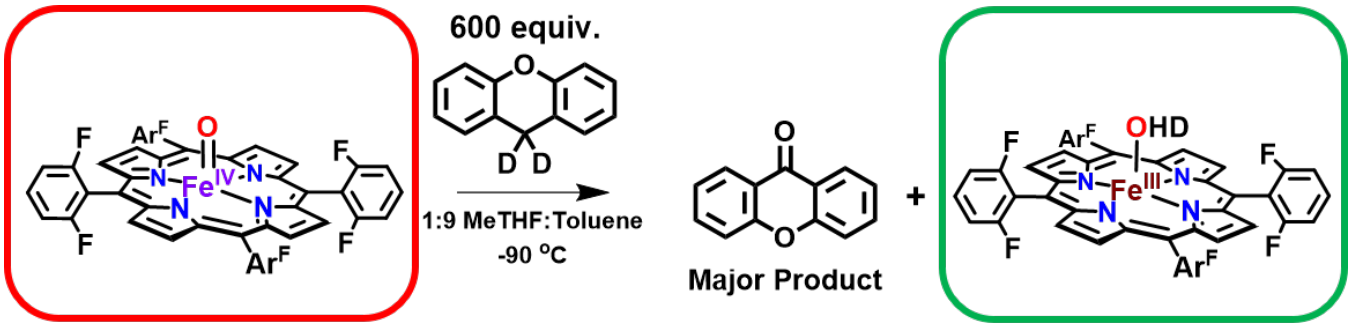

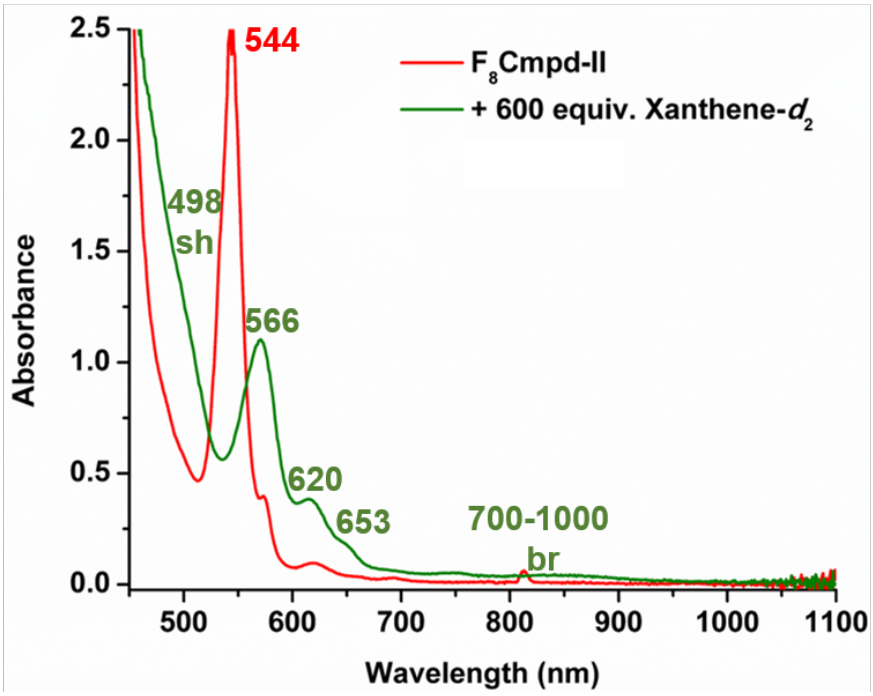

Figure S7. UV-vis monitoring of the addition of 600 equiv. xanthene-d_2 to F_8Cmpd-II at 0.1 mM at -90 °C in 1:9 MeTHF:toluene, resulting in the formation of the ferric aqua species (**red** to **green**). Great excess of xanthene-d_2 was needed (along with several hours, >10 hours) for full consumption of F_8Cmpd-II due to the extremely slow nature of the reaction.

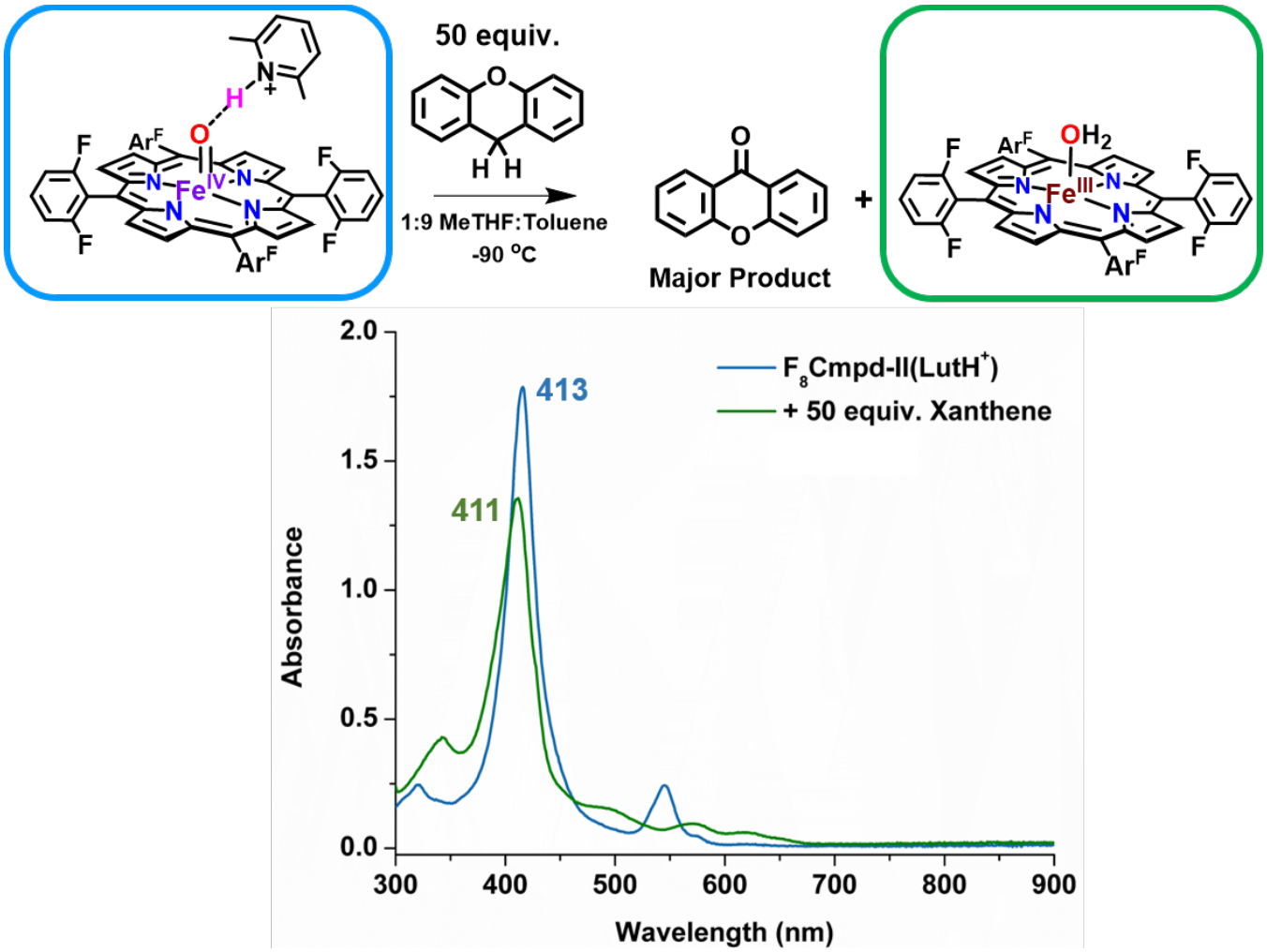

Figure S8. UV-vis monitoring of the addition of 50 equiv. xanthene to F_8Cmpd-II(LutH$^+$) at 0.01 mM at -90 °C in 1:9 MeTHF:toluene, resulting in the formation of the ferric aqua species (**blue** to **green**).

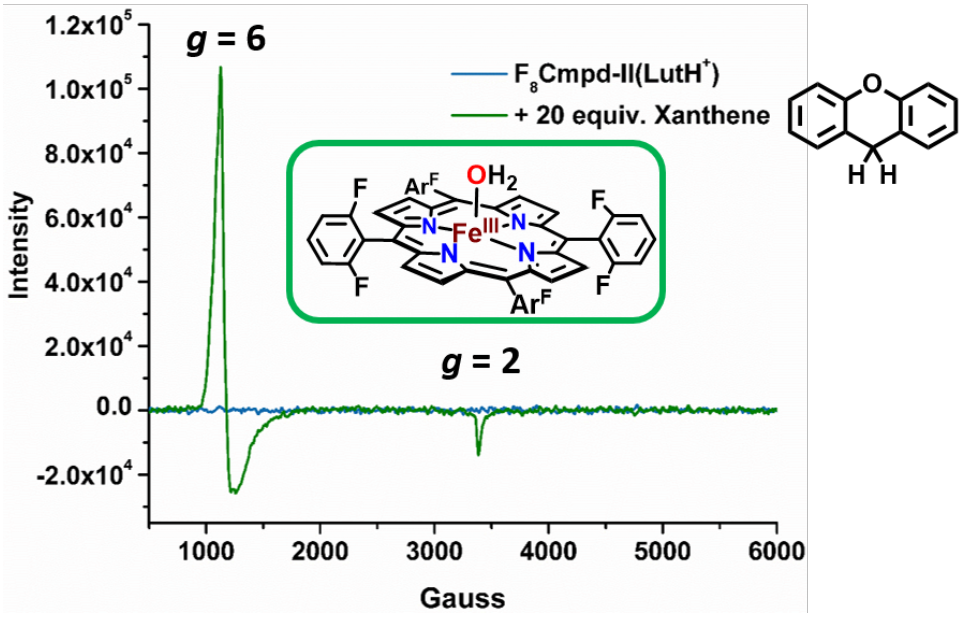

Figure S9. EPR spectra following the addition of 20 equiv. xanthene to F_8Cmpd-II(LutH$^+$) at 2 mM in 1:9 MeTHF:toluene at -90 ºC, resulting in the formation of the ferric aqua species (**blue** to **green**). The reaction was allowed to react for an hour before freezing the solution and acquiring an EPR spectrum at 10 K.

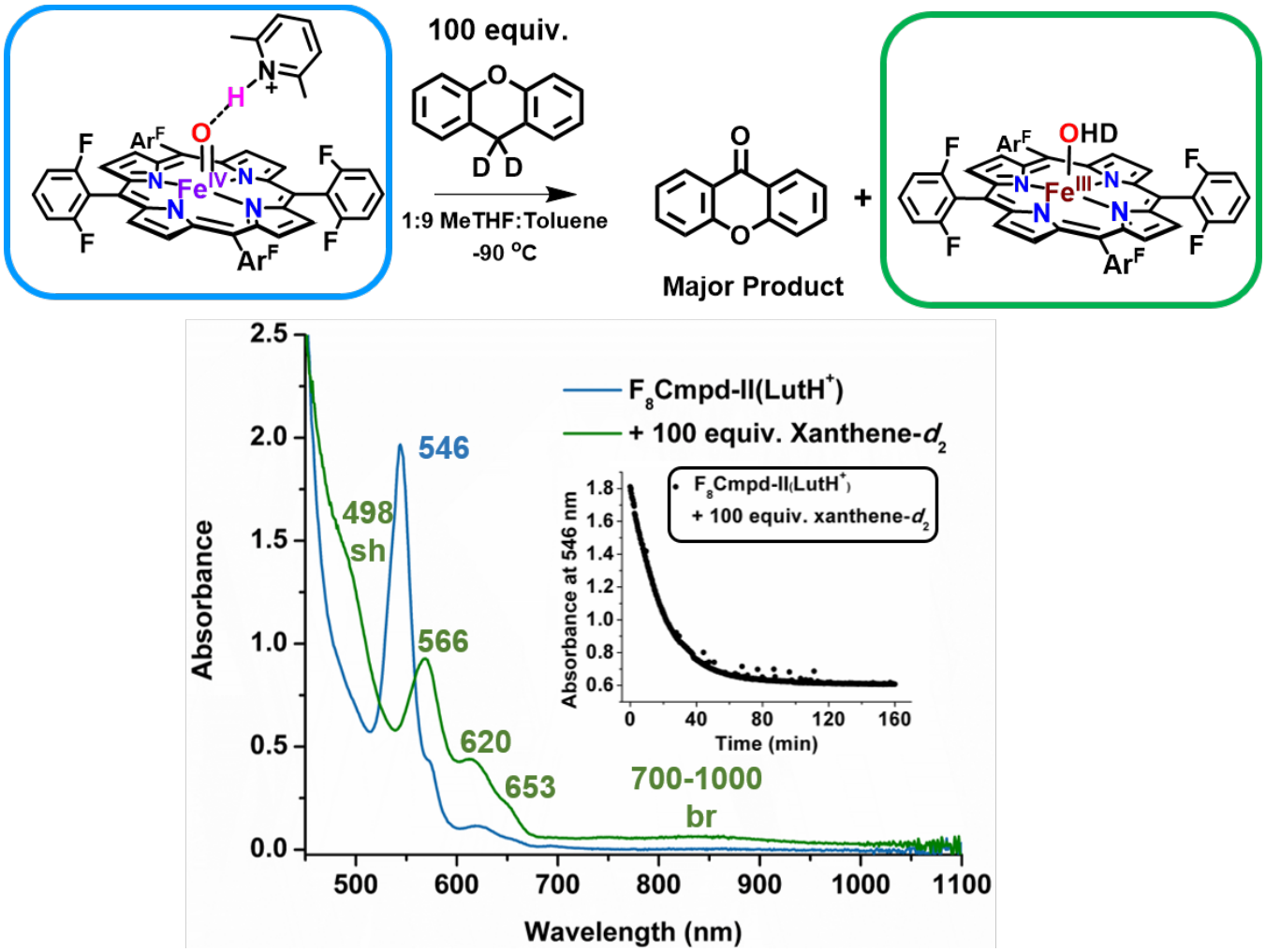

Figure S10. UV-vis monitoring of the addition of 100 equiv. xanthene-d_2 to F_8Cmpd-II(LutH$^+$) at 0.1 mM at -90 °C in 1:9 MeTHF:toluene, resulting in the formation of the ferric aqua species (**blue** to **green**). Inset: Decrease in the absorbance at 546 nm over time.

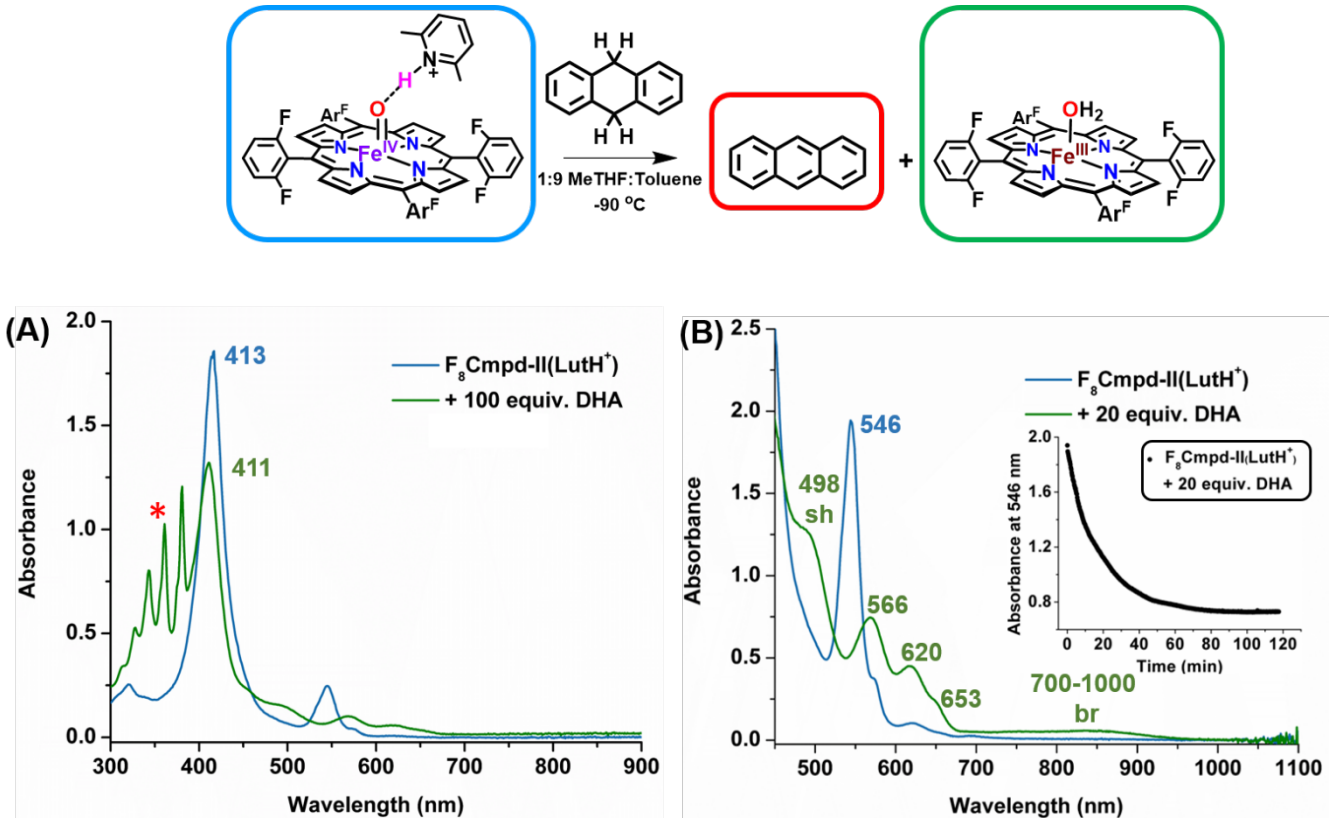

Figure S11. UV-vis monitoring of the addition of 9,10-dihydroanthracene (DHA) to F_8Cmpd-II(LutH$^+$) at 0.01 mM (**A**) and 0.1 mM (**B**) at -90 °C in 1:9 MeTHF:toluene, resulting in the formation of the ferric aqua species (**blue** to **green**). Inset: Decrease in the absorbance at 546 nm over time. It is of note that at 0.01 mM (**A**), the characteristic 5 sharp lined UV-vis signature between 300 - 380 nm denoted with a red asterisk grew in over time and is ascribed to the dehydrogenation of DHA over time by the high valent oxidant to anthracene.

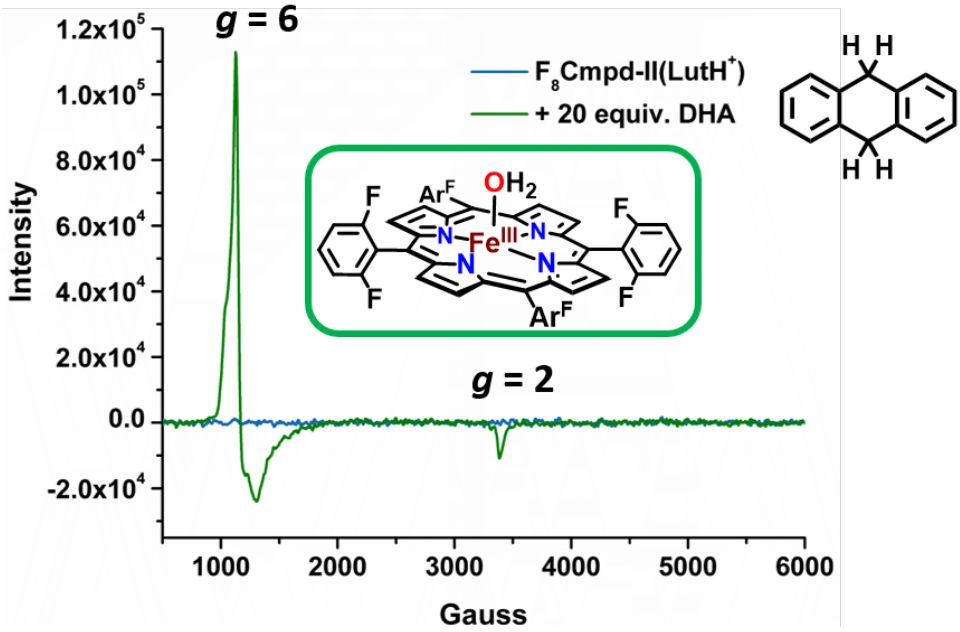

Figure S12. EPR spectra following the addition of 20 equiv. DHA to F_8Cmpd-II(LutH$^+$) at 2 mM in 1:9 MeTHF:toluene at -90 ^{o}C, resulting in the formation of the ferric aqua species (**blue** to **green**). The reaction was allowed to react for an hour before freezing the solution and acquiring an EPR spectrum at 10 K.

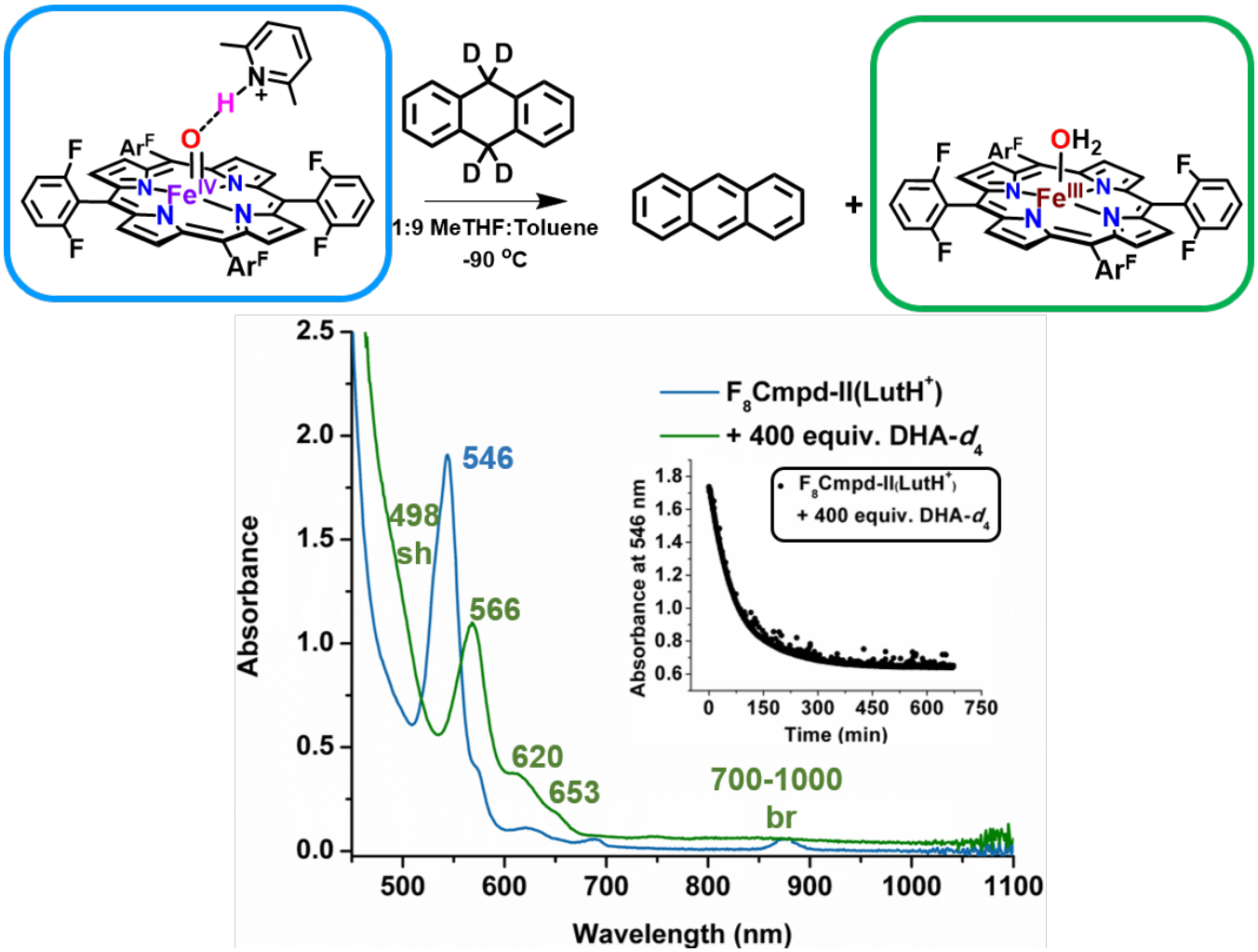

Figure S13. UV-vis monitoring of the addition of DHA-d_4 to F_8Cmpd-II(LutH$^+$) at 0.1 mM at -90 °C in 1:9 MeTHF:toluene, resulting in the formation of the ferric aqua species (**blue** to **green**). Inset: Decrease in the absorbance at 546 nm over time.

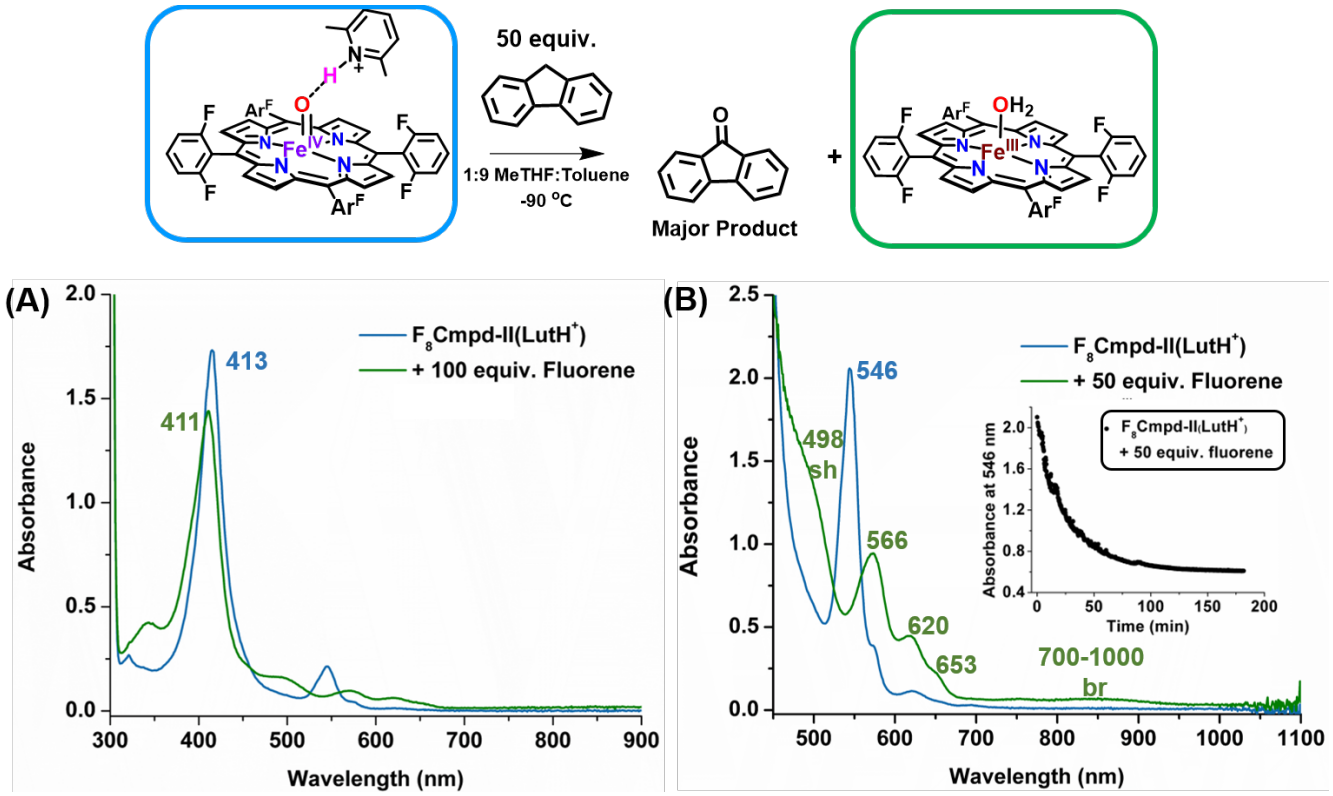

Figure S14. UV-vis monitoring of the addition of fluorene to F_8Cmpd-II(LutH$^+$) at 0.01 mM (**A**) and 0.1 mM (**B**) at -90 °C in 1:9 MeTHF:toluene, resulting in the formation of the ferric aqua species (**blue** to **green**). Inset: Decrease in the absorbance at 546 nm over time.

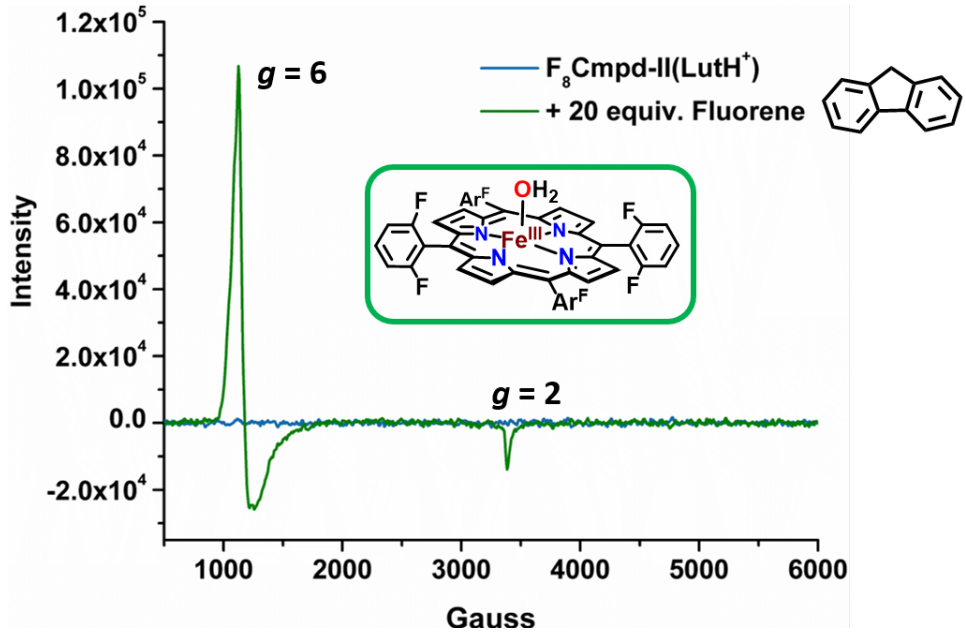

Figure S15. EPR spectra following the addition of 20 equiv. fluorene to F_8Cmpd-II(LutH$^+$) at 2 mM in 1:9 MeTHF:toluene at -90 °C, resulting in the formation of the ferric aqua species (**blue**

to **green**). The reaction was allowed to react for an hour before freezing the solution and acquiring an EPR spectrum at 10 K.

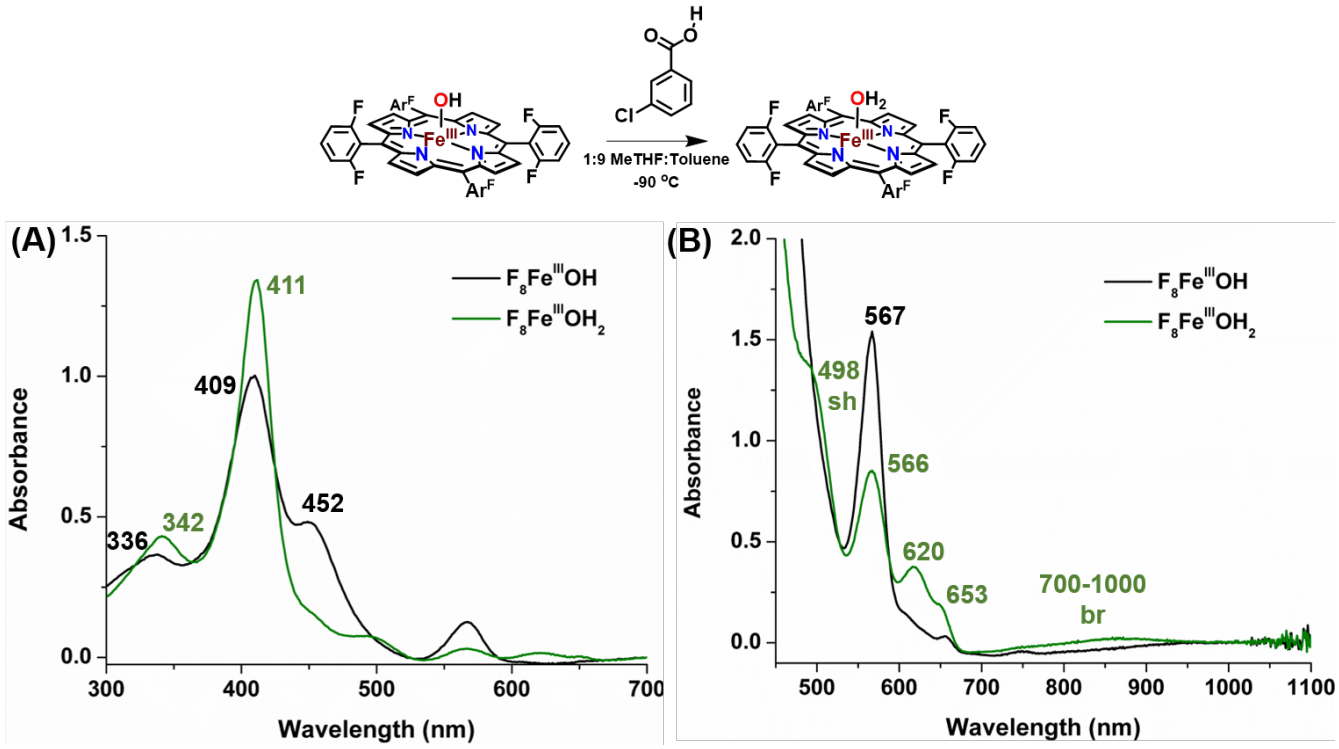

Figure S16. UV-vis monitoring of the addition of 1 equivalent 3-chlorobenzoic acid (the byproduct of the oxidant *m*CPBA used to generate the high valent complexes) to $F_8Fe^{III}OH$ at 0.01 mM (**A**) and 0.1 mM (**B**) at -90 °C in 1:9 MeTHF:toluene, resulting in the formation of the ferric aqua species (**black** to **green**). Thus, it can be suggested that when F_8Cmpd-II abstracts a hydrogen atom from various C–H substrates forming $F_8Fe^{III}OH$, that an additional proton may come from 3-chlorobenzoic acid (thereby protonating $F_8Fe^{III}OH$ and forming the ferric aqua species observed at the end of the reaction between the high valent species and various C–H substrates).

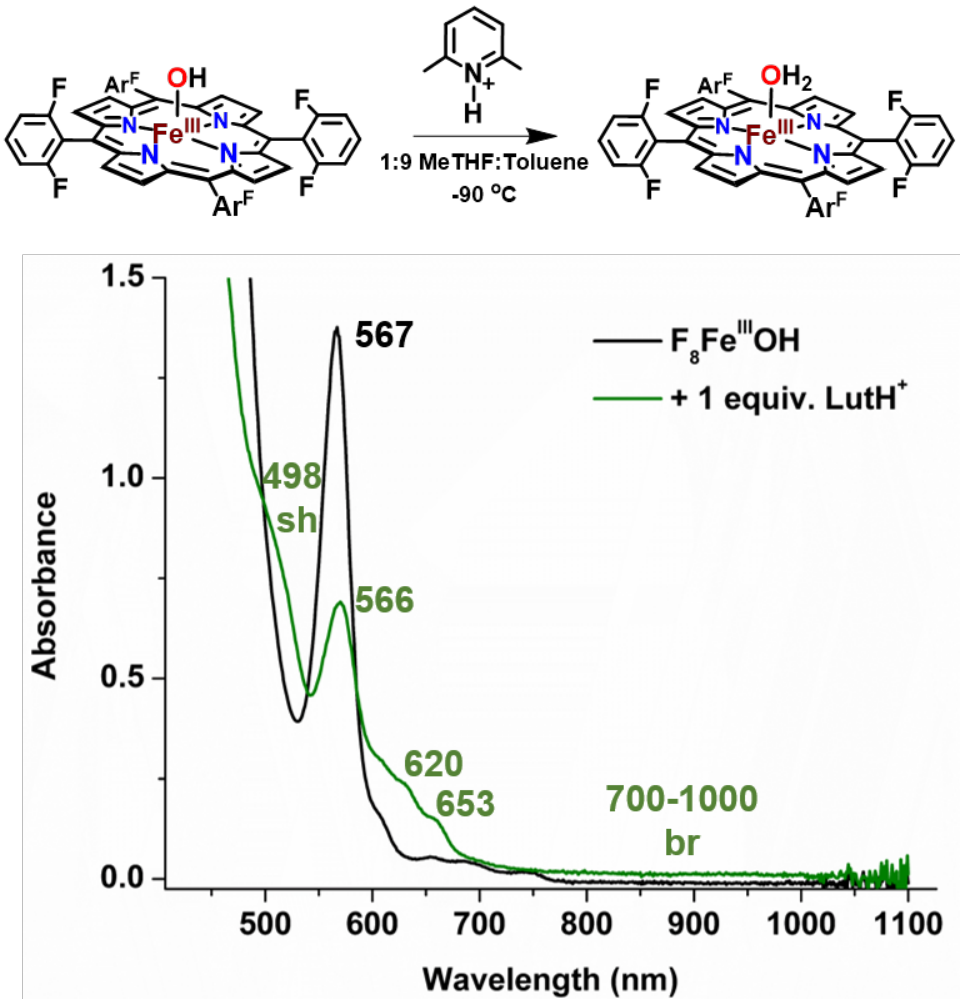

Figure S17. UV-vis monitoring of the addition of 1 equivalent 2,6-lutidinium triflate ($LutH^+$) to $F_8Fe^{III}OH$ at 0.1 mM at -90 °C in 1:9 MeTHF:toluene, resulting in the formation of the ferric aqua species (**black** to **green**). Thus, it can be suggested that when F_8Cmpd-II($LutH^+$) abstracts a hydrogen atom from various C–H substrates forming $F_8Fe^{III}OH$, that an additional proton may come from the Lewis acid that is hydrogen bonded to the oxo ligand (thereby protonating $F_8Fe^{III}OH$ and forming the ferric aqua species observed at the end of the reaction between the high valent species and various C–H substrates).

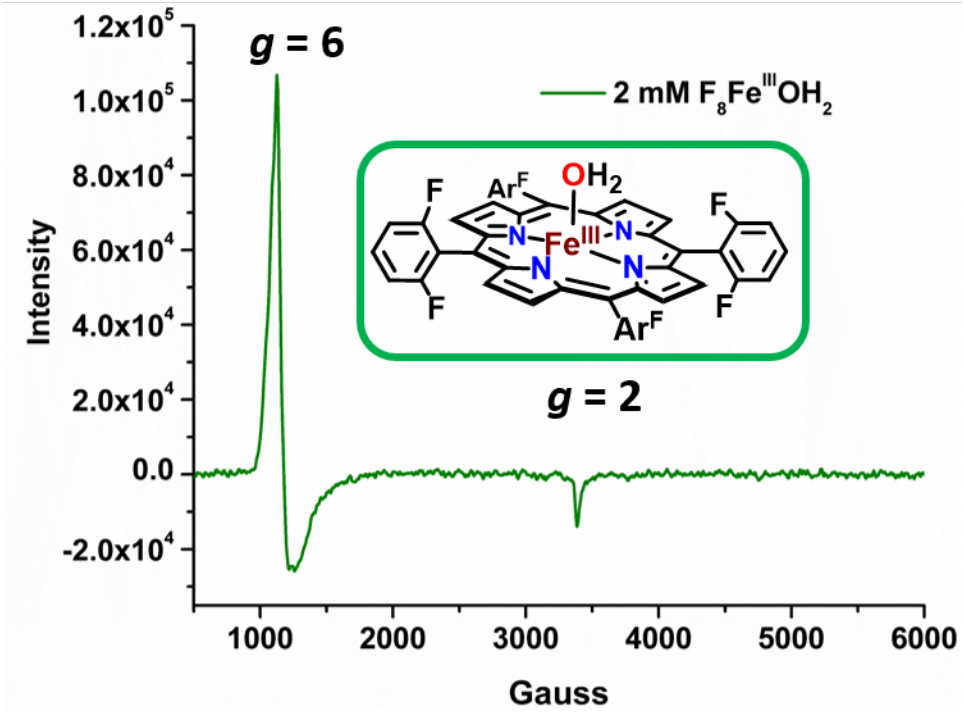

Figure S18. EPR spectrum following the addition of 1 equiv. 3-chlorobenzoic acid to $F_8Fe^{III}OH$ at 2 mM in 1:9 MeTHF:toluene at -90 °C yielding the g = 6 and g= 2 signals ascribed to the high-spin ferric species, $F_8Fe^{III}OH_2$.

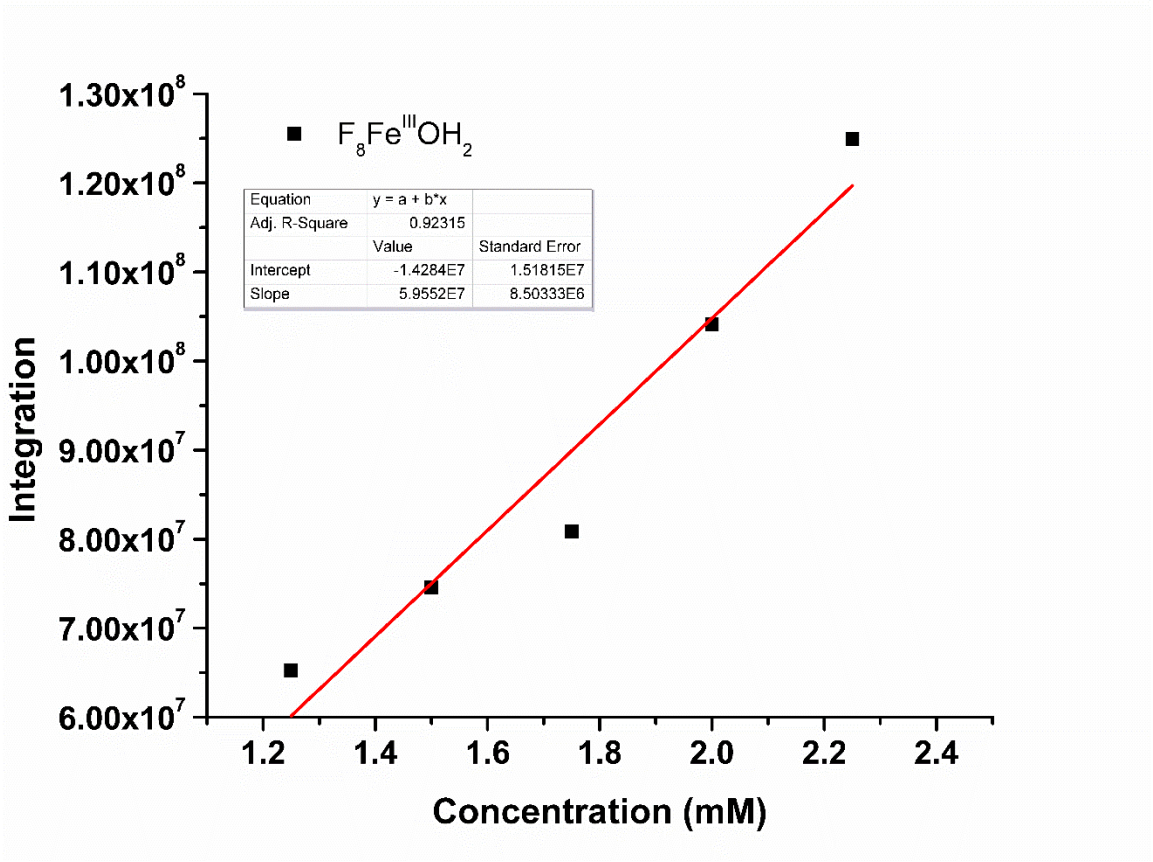

Figure S19. EPR spectra following the addition of 1 equiv. 3-chlorobenzoic acid to $F_8Fe^{III}OH$ at 1.25, 1.5, 1.75, 2, 2.25 mM in 1:9 MeTHF:toluene at -90 °C. The resulting species were doubly integrated and plotted versus the various concentrations.

Table S1. EPR spectra following the addition of 1 equiv. 3-chlorobenzoic acid to $F_8Fe^{III}OH$ at 1.25, 1.5, 1.75, 2, 2.25 mM in 1:9 MeTHF:toluene at -90 °C. The resulting species were doubly integrated and plotted versus the various concentrations.

Concentration of $F_8Fe^{III}OH_2$ (mM)	**Double Integration of the g ~ 6.0 EPR signal**
1.25	$6.52x10^7$
1.5	$7.46x10^7$
1.75	$8.09x10^7$
2	$1.04x10^8$
2.25	$1.25x10^8$

Table S2. EPR spectroscopy following the addition of 20 equiv. of various C–H substrates to F_8Cmpd-II or F_8Cmpd-II(LutH$^+$) at 2 mM 1:9 MeTHF:toluene at -90 °C and allowed to subsequently react for one hour. All reactions resulted in a g = 6 and g = 2 signal ascribed to a high spin ferric species. The yield of the ferric species was quantified by comparision of the integration of the ferric species with a standard curve of the independently generated product by EPR spectroscopy.

Reaction	**Double Integration of the g ~ 6.0 EPR signal**	**% yield of $F_8Fe^{III}OH_2$ at end of reaction**
F_8Cmpd-II + 20 equiv. Xanthene + 1 hr	1.00×10^8	96%
F_8Cmpd-II(LutH$^+$) + 20 equiv. Xanthene + 1 hr	1.01×10^8	97%
F_8Cmpd-II(LutH$^+$) + 20 equiv. DHA + 1 hr	1.02×10^8	98%
F_8Cmpd-II(LutH$^+$) + 20 equiv. Fluorene + 1 hr	1.01×10^8	97%

III. Kinetic trials via UV-vis spectroscopy determining the second order rate constants (k_2) of C–H cleavage.

Pseudo-first-order rate plots were performed by observing the disappearance of the 544 (for F_8Cmpd-II) or 546 (for F_8Cmpd-II(LutH$^+$)) nm band to obtain plots of $\ln[(A_t - A_f)/(A_i - A_f)]$ versus time (seconds), which were found to be linear for three or more half-lives. Second-order rate plots (k_{obs} vs. [substrate]) were obtained using averages and standard deviations from three trials at each concentration of substrate. All kinetic experiments were run with 0.1 mM F_8Cmpd-II or F_8Cmpd-II(LutH$^+$) at –90 °C in 1:9 MeTHF:toluene. The method of initial rates was used to determine the observed rate constants.

A. F_8Cmpd-II and Xanthene

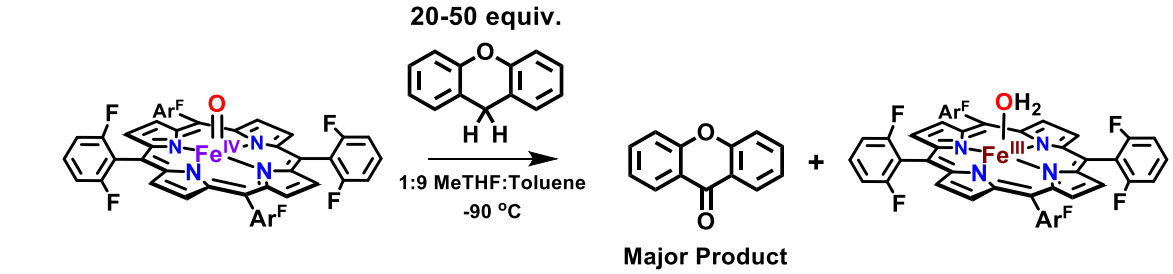

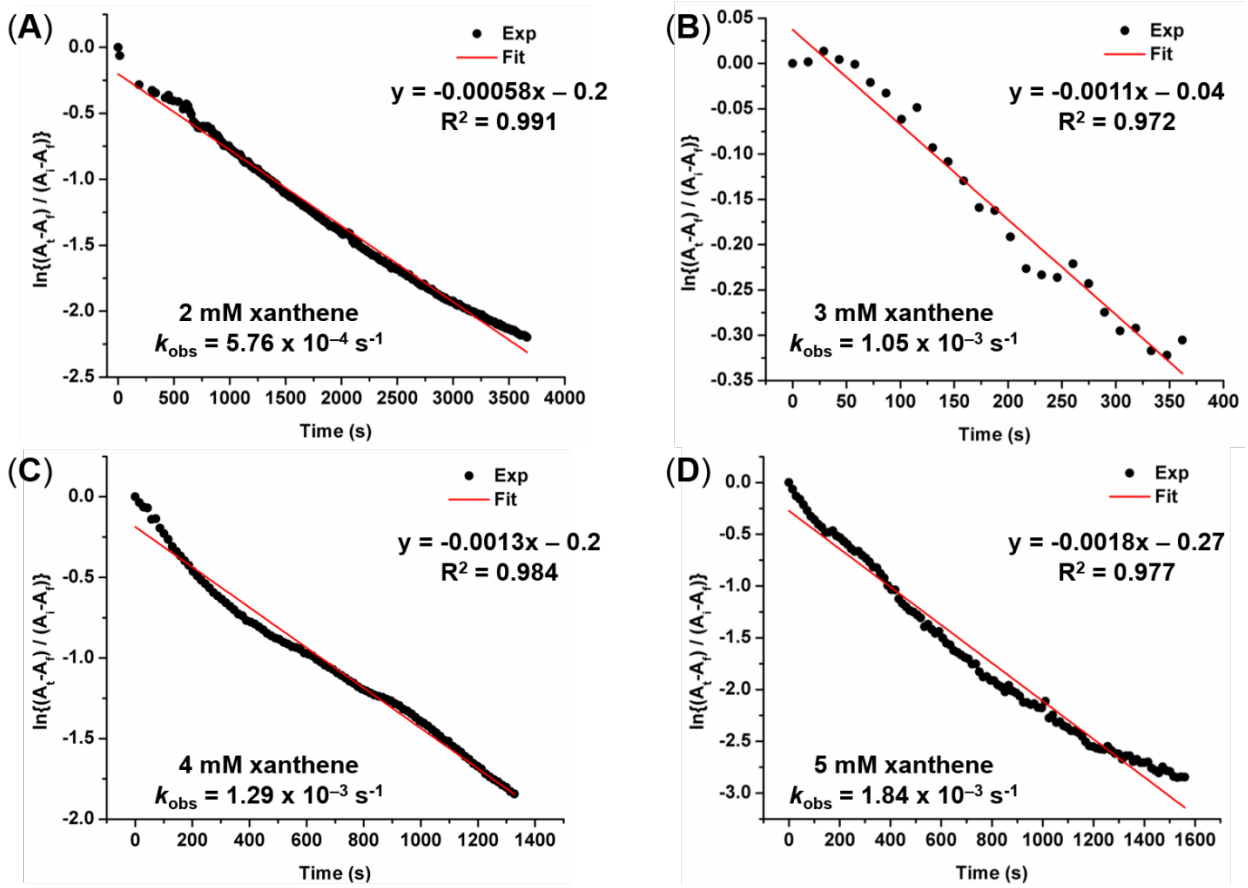

Figure S20. UV-vis spectroscopy monitoring the rate of reaction upon addition of (**A**) 20, (**B**) 30 (**C**) 40, and (**D**) 50 equiv. of xanthene to F_8Cmpd-II.

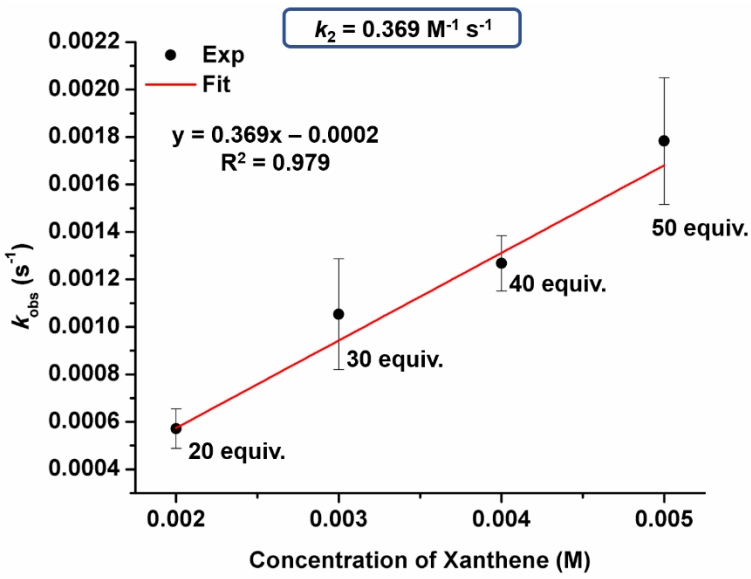

Figure S21. Second-order rate constant determined under pseudo-first-order conditions of the addition of xanthene to F_8Cmpd-II, giving k_2 = 0.369 ± 0.031 M^{-1} s^{-1}. Each data point is an average of three trials. The error bars are representing the standard deviation.

Table S3. Average and standard deviation for k_{obs} of the reaction between F_8Cmpd-II (0.1 mM) and xanthene. Three trials were run for each concentration of xanthene.

Concentration of Xanthene (M)	Average k_{obs} (s^{-1})	Standard Deviation of k_{obs}
0.002	5.72 x 10^{-4}	8.33 x 10^{-5}
0.003	1.05 x 10^{-3}	2.33 x 10^{-4}
0.004	1.27 x 10^{-3}	1.17 x 10^{-4}
0.005	1.78 x 10^{-3}	2.67 x 10^{-4}

B. F_8Cmpd-II(LutH$^+$) and Xanthene

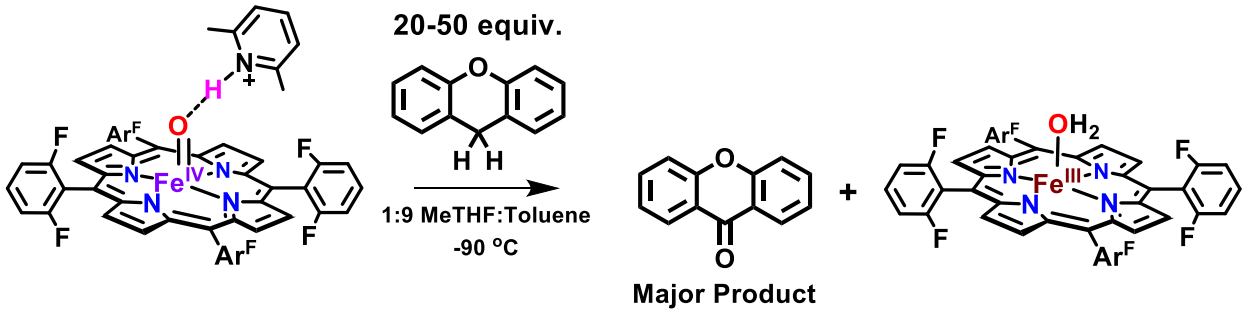

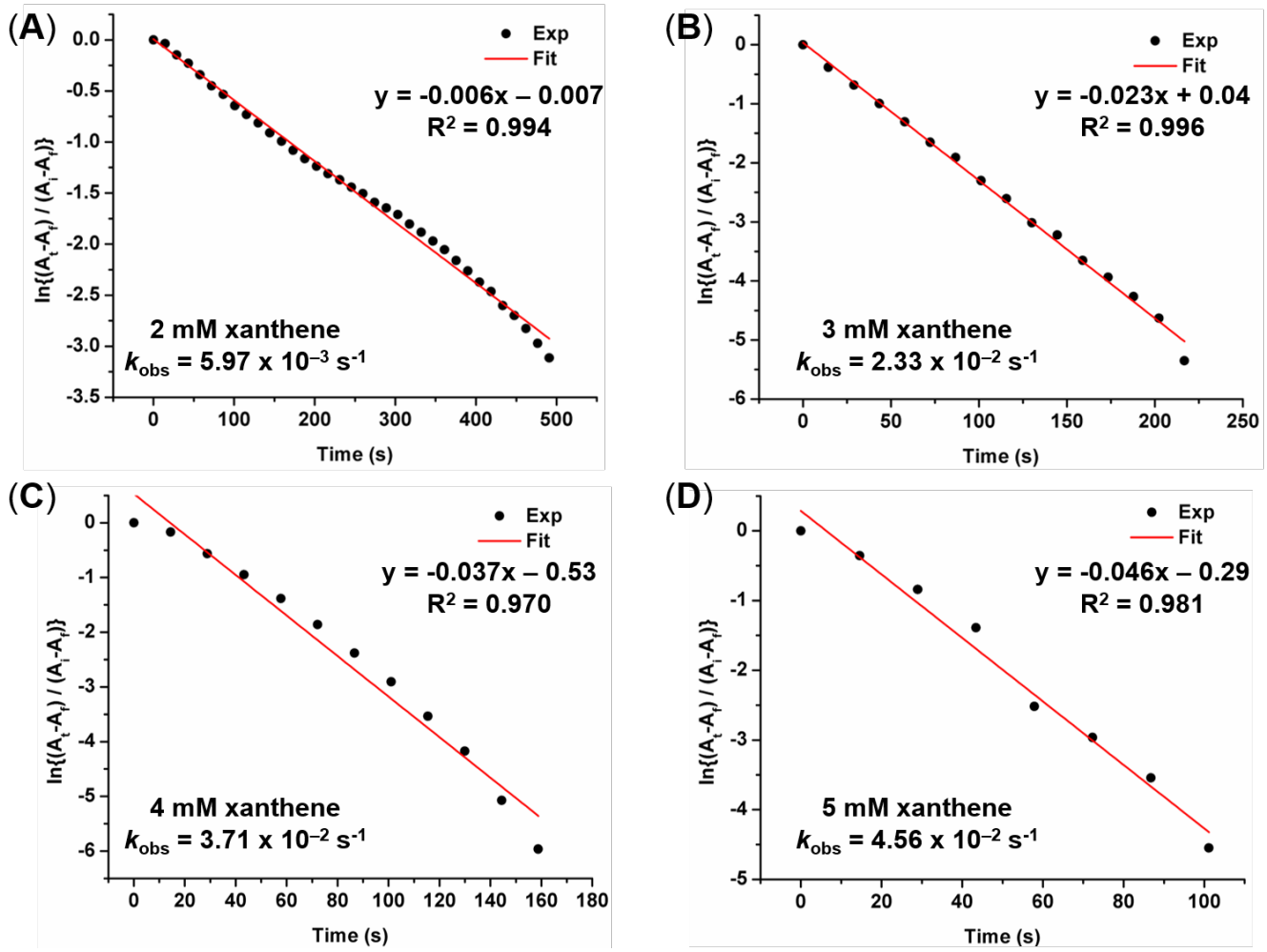

Figure S22. UV-vis spectroscopy monitoring the rate of reaction upon addition of (**A**) 20, (**B**) 30 (**C**) 40, and (**D**) 50 equiv. of xanthene to F_8Cmpd-II(LutH$^+$).

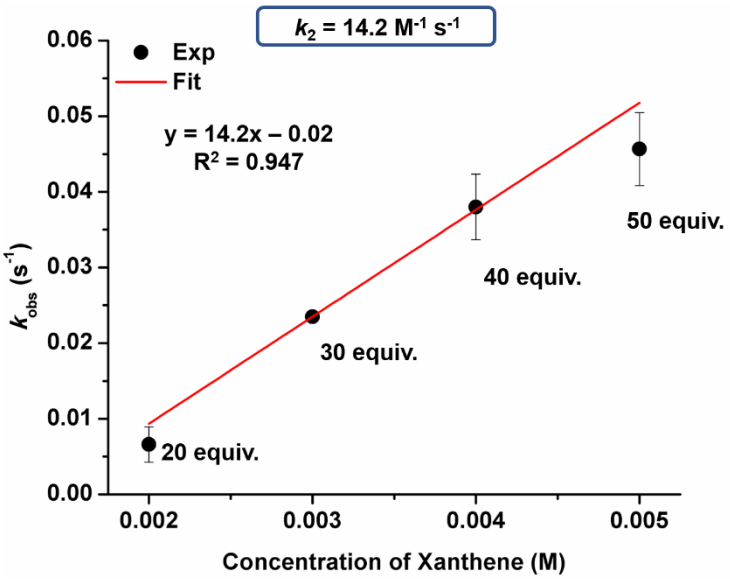

Figure S23. Second-order rate constant determined under pseudo-first-order conditions of the addition of xanthene to F_8Cmpd-II(LutH$^+$), giving k_2 = 14.2 ± 1.9 M^{-1} s^{-1}. Each data point is an average of three trials. The error bars are representing the standard deviation.

Table S4. Average and standard deviation for k_{obs} of the reaction between F_8Cmpd-II(LutH$^+$) and xanthene. Three trials were run for each concentration of xanthene.

Concentration of Xanthene (M)	Average k_{obs} (s^{-1})	Standard Deviation of k_{obs}
0.002	6.60 x 10^{-3}	2.33 x 10^{-3}
0.003	2.35 x 10^{-2}	1.17 x 10^{-4}
0.004	3.80 x 10^{-2}	4.33 x 10^{-3}
0.005	4.57 x 10^{-2}	4.83 x 10^{-3}

C. F_8Cmpd-II(LutH$^+$) and 9,10-dihydroanthracene

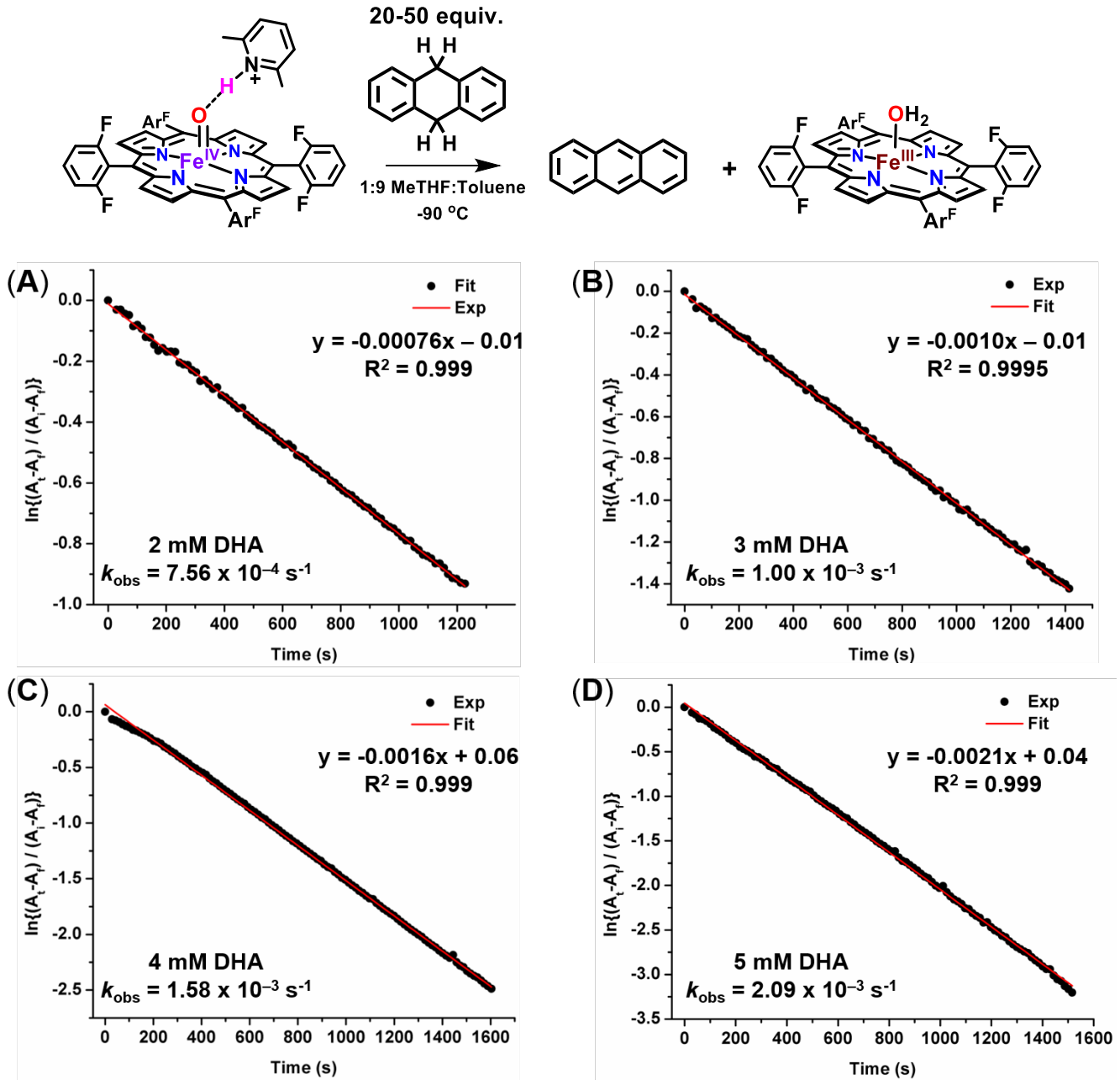

Figure S24. UV-vis spectroscopy monitoring the rate of reaction upon addition of (**A**) 20, (**B**) 30, (**C**) 40, and (**D**) 50 equiv. of 9,10-dihydroanthracene to F_8Cmpd-II(LutH$^+$).

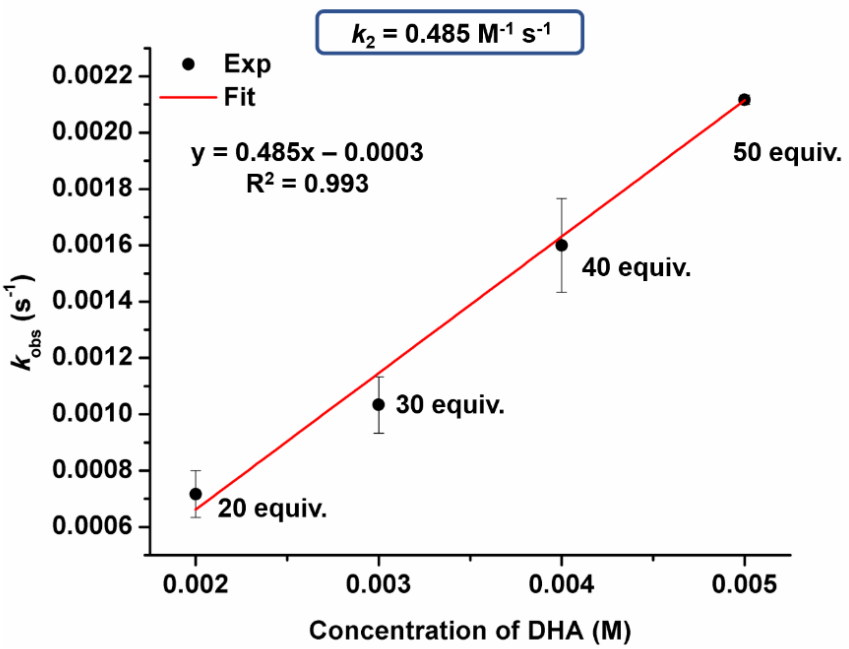

Figure S25. Second order rate constant k_2 determined under pseudo first order conditions of the addition of 9,10-dihydroanthracene to F_8Cmpd-II(LutH$^+$), giving a k_2 = 0.485 ± 0.02 M^{-1} s^{-1}. Each data point is an average of three trials. The error bars are representing the standard deviation.

Table S5. Average and standard deviation for k_{obs} of the reaction between F_8Cmpd-II(LutH$^+$) and DHA. Three trials were run for each concentration of DHA.

Concentration of DHA (M)	Average k_{obs} (s^{-1})	Standard Deviation of k_{obs}
0.002	7.17 x 10^{-4}	8.33 x 10^{-5}
0.003	1.03 x 10^{-3}	1.00 x 10^{-4}
0.004	1.60 x 10^{-3}	1.67 x 10^{-4}
0.005	2.12 x 10^{-3}	1.67 x 10^{-5}

D. F_8Cmpd-II(LutH$^+$) and Fluorene

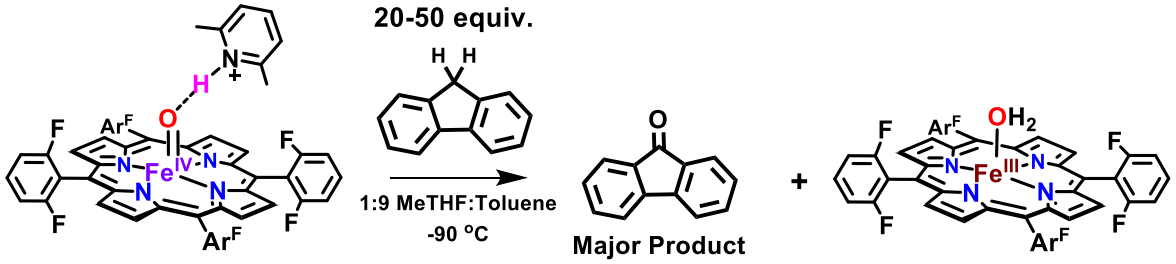

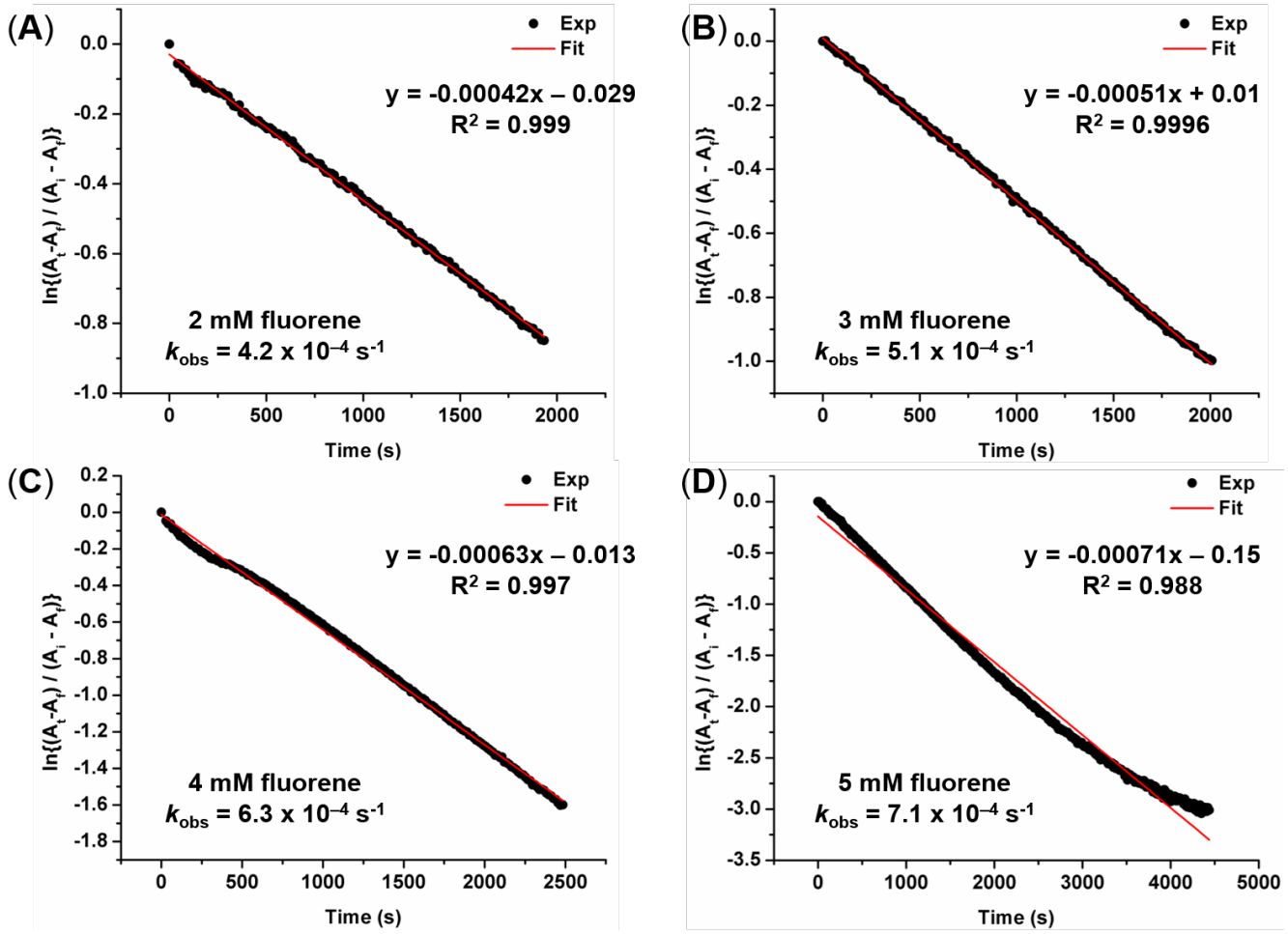

Figure S26. UV-vis spectroscopy monitoring the rate of reaction upon addition of (**A**) 20, (**B**) 30, (**C**) 40, and (**D**) 50 equiv. of fluorene to F_8Cmpd-II(LutH$^+$).

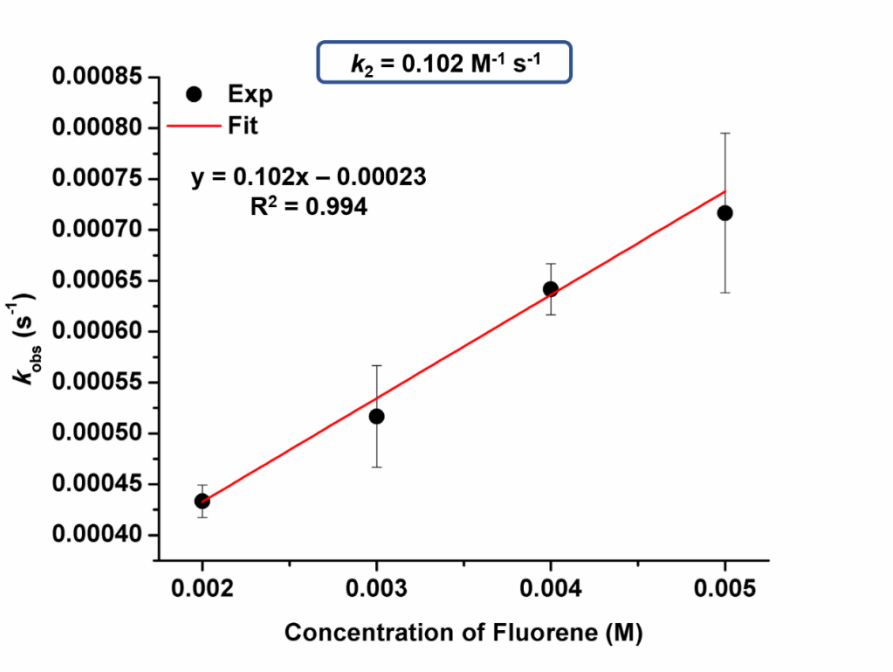

Figure S27. Second order rate constant k_2 determined under pseudo first order conditions of the addition of fluorene to F_8Cmpd-II(LutH$^+$), giving a k_2 = 0.102 ± 0.005 M^{-1} s^{-1}. Each data point is an average of three trials. The error bars are representing the standard deviation.

Table S6. Average and standard deviation for k_{obs} of the reaction between F_8Cmpd-II(LutH$^+$) and fluorene. Three trials were run for each concentration of fluorene.

Concentration of Fluorene (M)	Average k_{obs} (s^{-1})	Standard Deviation of k_{obs}
0.002	4.33 x 10^{-4}	1.58 x 10^{-5}
0.003	5.17 x 10^{-4}	5.00 x 10^{-5}
0.004	6.42 x 10^{-4}	2.50 x 10^{-5}
0.005	7.17 x 10^{-4}	7.83 x 10^{-5}

IV. Kinetic trials via UV-vis spectroscopy determining the second order rate constants (k_2) of C–D cleavage and thus the kinetic isoptope effects (KIE).

A. F_8Cmpd-II and Xanthene-d_2

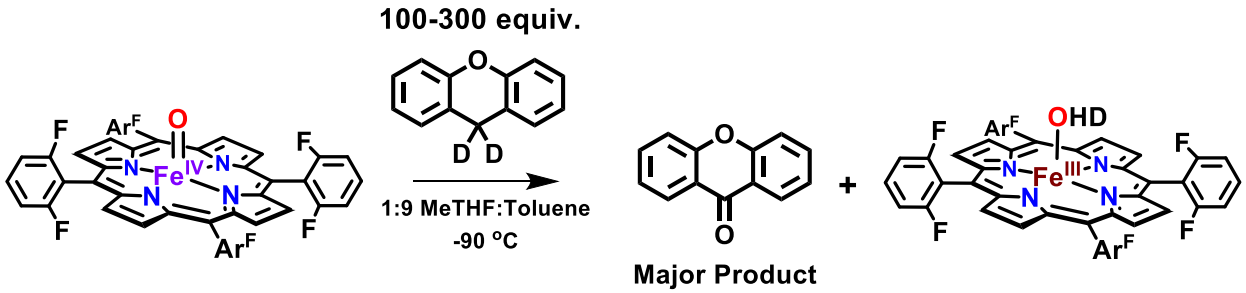

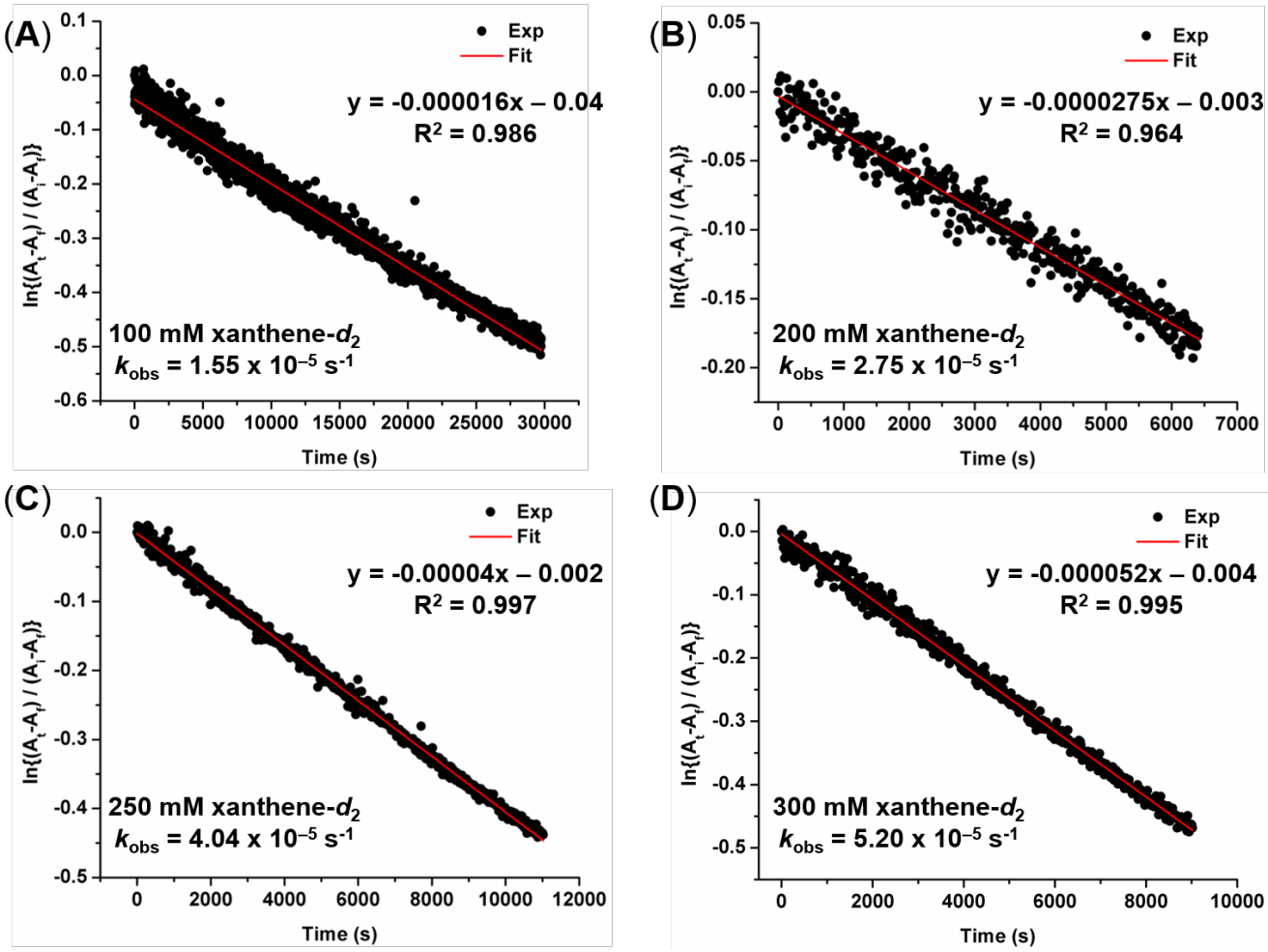

Figure S28. UV-vis spectroscopy monitoring the rate of reaction upon addition of (**A**) 100, (**B**) 200, (**C**) 250, and (**D**) 300 equiv. of xanthene-d_2 to F_8Cmpd-II.

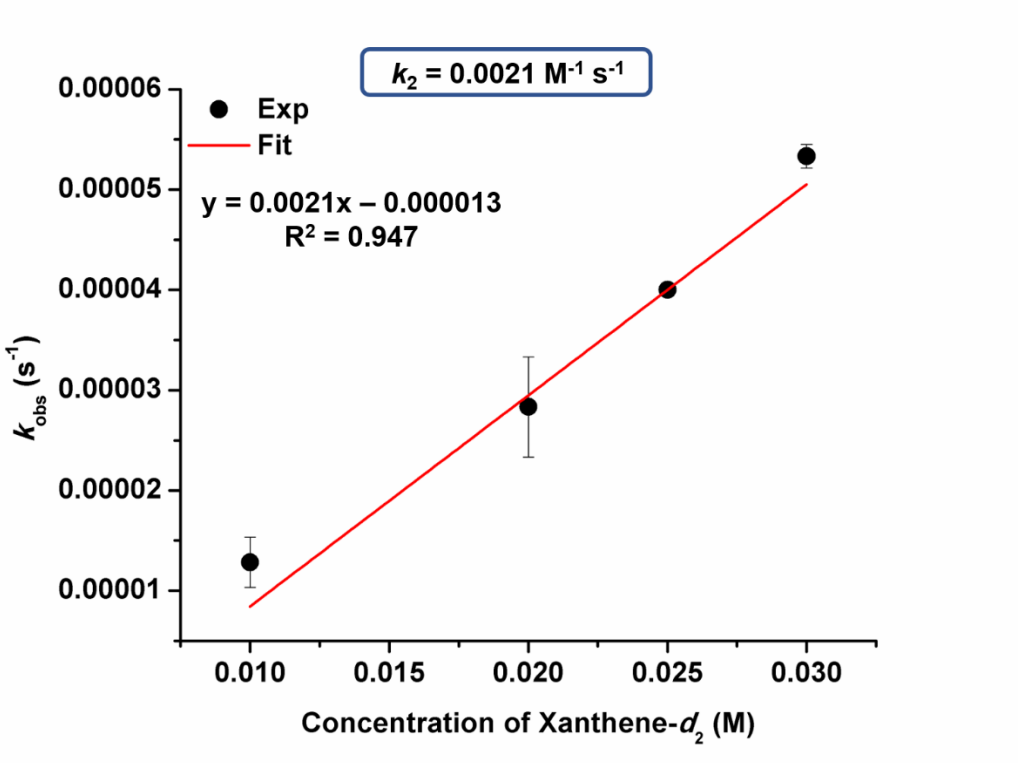

Figure S29. Second order rate constant k_2 determined under pseudo first order conditions of the addition of xanthene-d_2 to F_8Cmpd-II, giving a k_2 = 0.0021 ± 0.0003 M^{-1} s^{-1}. Each data point is an average of three trials. The error bars are representing the standard deviation.

Table S7. Average and standard deviation for k_{obs} of the reaction between F_8Cmpd-II and xanthene-d_2. Three trials were run for each concentration of xanthene-d_2.

Concentration of Xanthene-d_2 (M)	Average k_{obs} (s^{-1})	Standard Deviation of k_{obs}
0.01	1.28 x 10^{-5}	2.50 x 10^{-6}
0.02	2.83 x 10^{-5}	5.00 x 10^{-6}
0.025	4.00 x 10^{-5}	1.33 x 10^{-8}
0.03	5.33 x 10^{-5}	1.17 x 10^{-6}

B. F_8Cmpd-II(LutH$^+$) and Xanthene-d_2

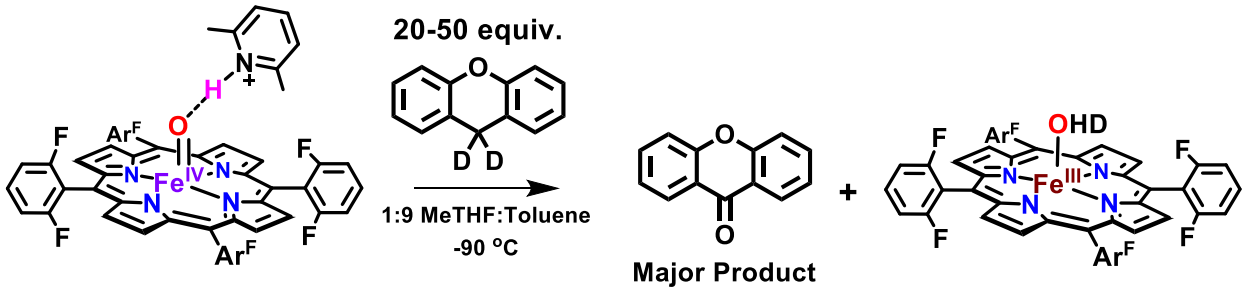

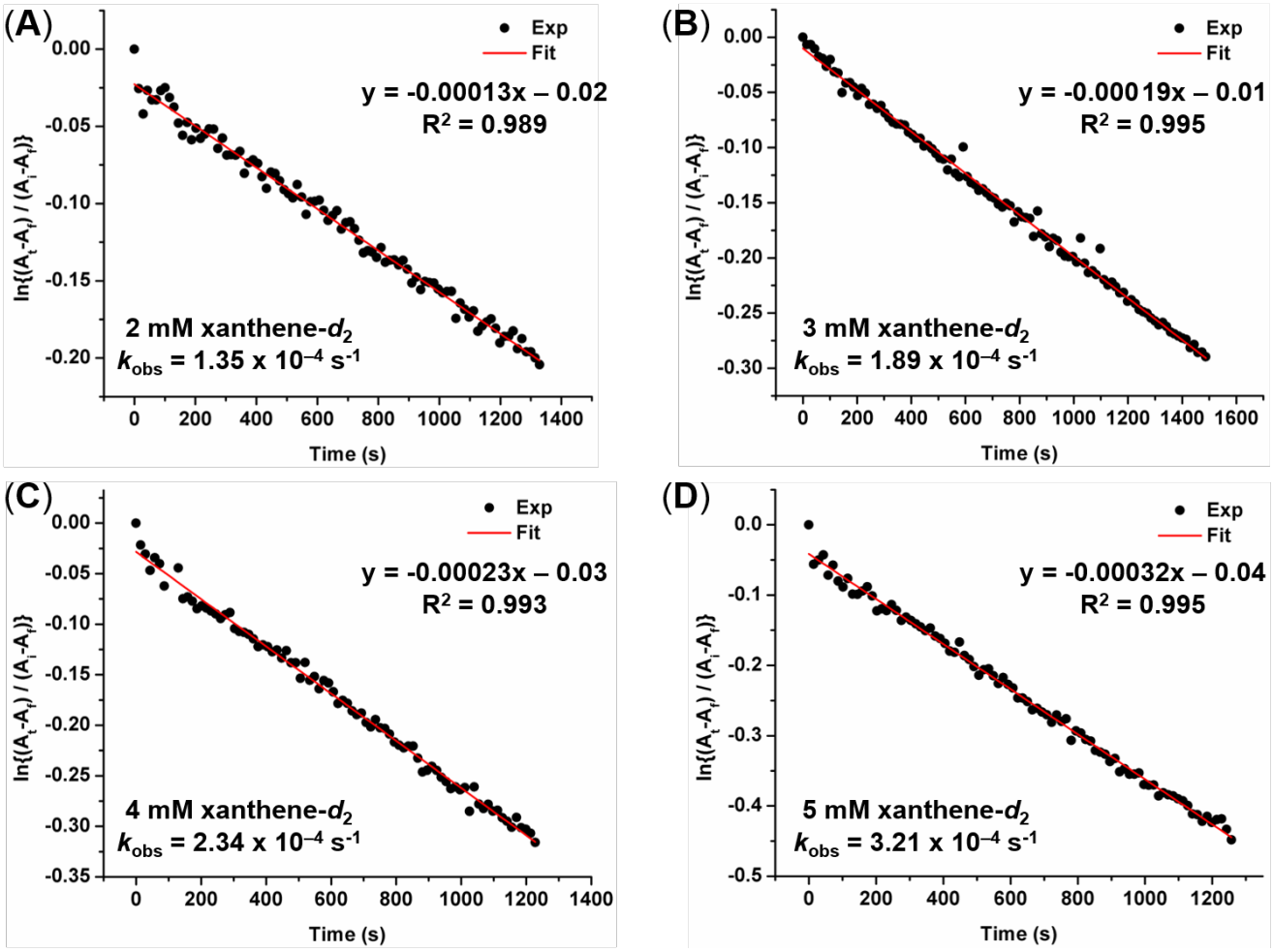

Figure S30. UV-vis spectroscopy monitoring the rate of reaction upon addition of (**A**) 20, (**B**) 30, (**C**) 40, and (**D**) 50 equiv. of xanthene-d_2 to F_8Cmpd-II(LutH$^+$).

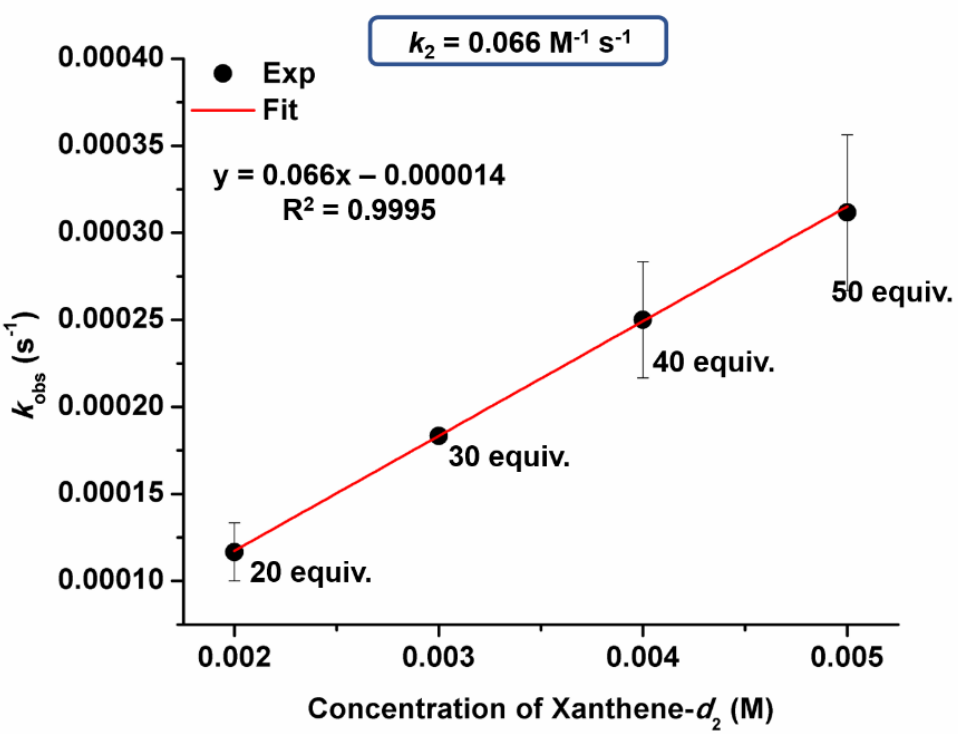

Figure S31. Overall second order rate constant determined under pseudo first order conditions of the addition of xanthene-d_2 to F_8Cmpd-II(LutH$^+$), giving a k_2 = 0.0659 ± 0.0008 M^{-1} s^{-1}. Each data point is an average of three trials. The error bars are representing the standard deviation.

Table S8. Average and standard deviation for k_{obs} of the reaction between F_8Cmpd-II(LutH$^+$) and xanthene-d_2. Three trials were run for each concentration of xanthene-d_2.

Concentration of Xanthene-d_2 (M)	Average k_{obs} (s^{-1})	Standard Deviation of k_{obs}
0.01	1.17 x 10^{-4}	1.67 x 10^{-5}
0.02	1.83 x 10^{-4}	1.00 x 10^{-6}
0.025	2.50 x 10^{-4}	3.33 x 10^{-5}
0.03	3.12 x 10^{-4}	4.48 x 10^{-5}

C. F_8Cmpd-II(LutH$^+$) and 9,10-dihydroanthracene-d_4

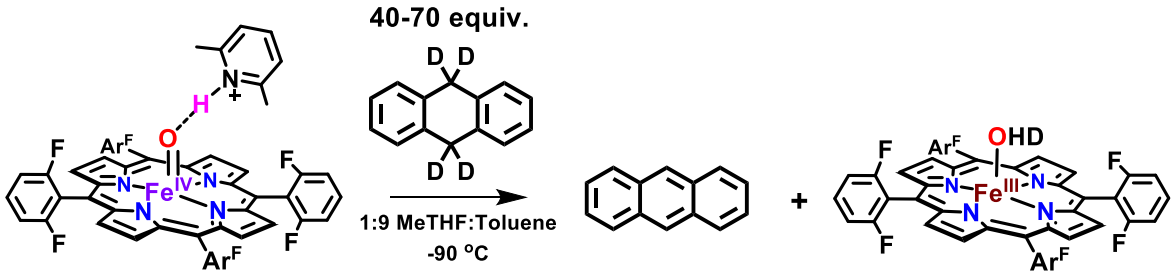

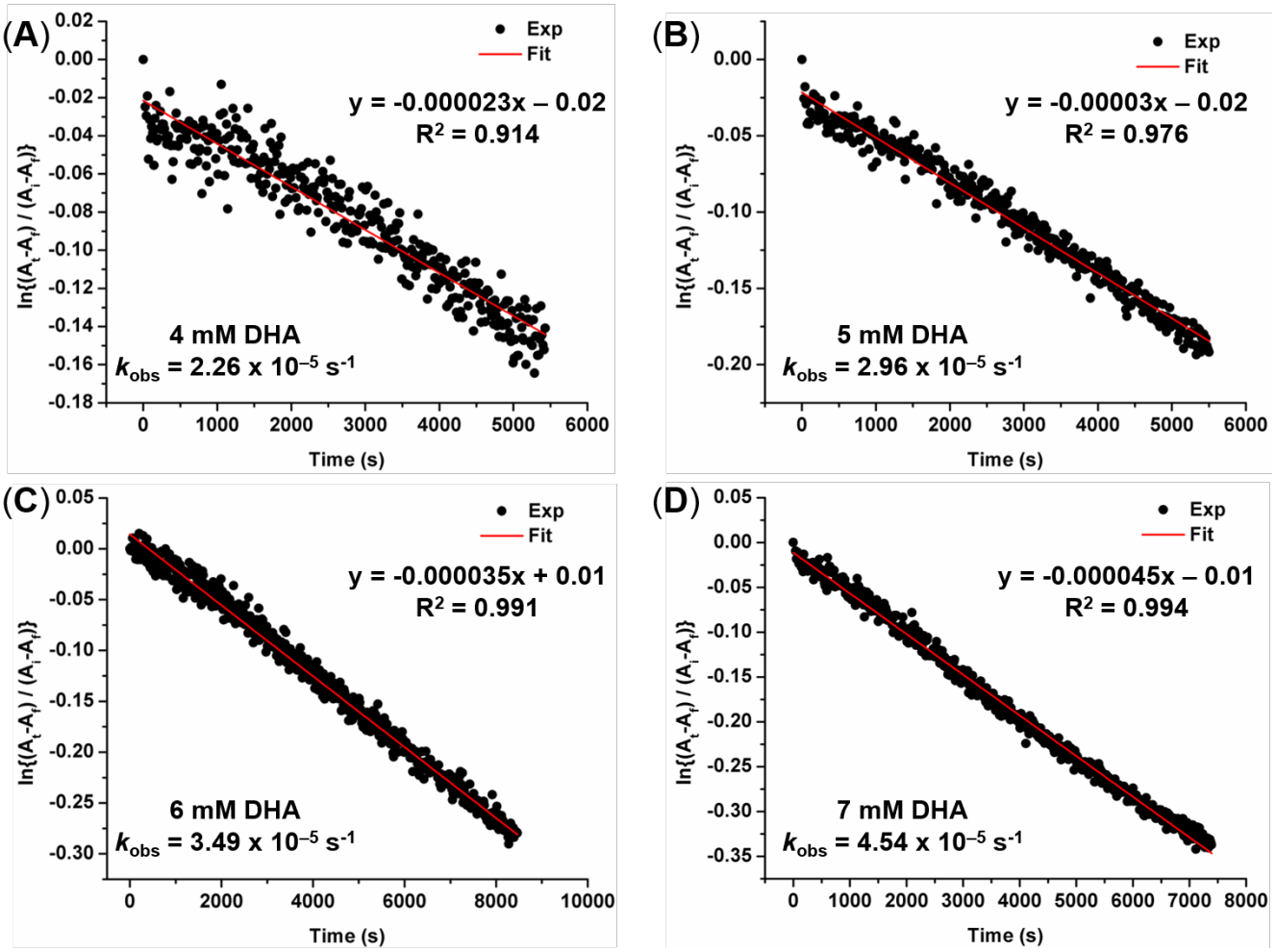

Figure S32. UV-vis spectroscopy monitoring the rate of reaction upon addition of (**A**) 40, (**B**) 50, (**C**) 60, and (**D**) 70 equiv. of DHA-d_4 to F_8Cmpd-II(LutH$^+$).

Table S9. Average and standard deviation for k_{obs} of the reaction between F_8Cmpd-II(LutH$^+$) and DHA-d_4. Three trials were run for each concentration of DHA-d_4.

Concentration of DHA-d_4 (M)	Average k_{obs} (s^{-1})	Standard Deviation of k_{obs}
0.004	2.17×10^{-5}	5.00×10^{-6}
0.005	2.67×10^{-5}	3.33×10^{-6}
0.006	3.33×10^{-5}	2.50×10^{-6}
0.007	4.00×10^{-5}	6.50×10^{-6}

Table S10. Second order rate constants (k_2, $M^{-1}s^{-1}$) of C–D cleavage by F_8Cmpd-II or F_8Cmpd-II(LutH$^+$) resulting in the determination of the kinetic isotope effect (k_H/k_D).

	F_8Cmpd-II	KIE (k_H/k_D)	F_8Cmpd-II(LutH$^+$)	KIE (k_H/k_D)
Xanthene-d_2	0.0021 M^{-1} s^{-1}	176 **	0.066 M^{-1} s^{-1}	215 **
DHA-d_4			0.006 M^{-1} s^{-1}	81 **

** These very large KIE quantities are only apparent values; with large KIE's, the amount of residual protium in the deuterated substrates (98 – 99 % D), which will thus react extremely rapidly, significantly diminishes the ability to accurately determine large KIE's. At the level of protium present, we can only say that the isotope effects here, marked with **, are KIE ~ 50. Also, see the text, 6th manuscript page and citation # 65. We are grateful to a reviewer of this article for guidance concerning this matter.

V. Kinetic trials via UV-vis spectroscopy determining the second order rate constant (k_2) of C–H cleavage of DHA with F_8Cmpd-II(LutD$^+$), and thus the kinetic isoptope effect (KIE).

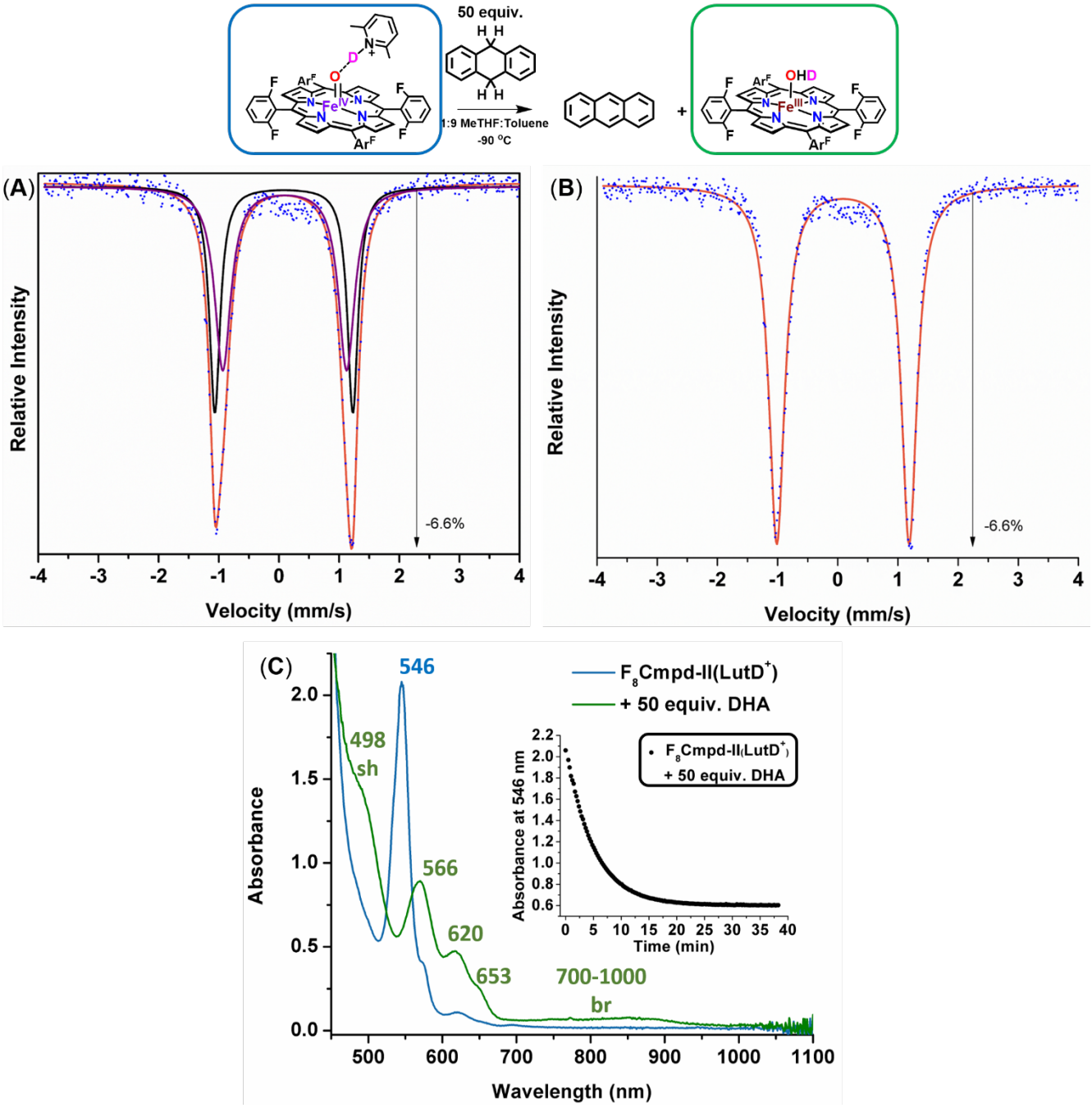

Figure S33. (**A and B**) Mössbauer spectrum of F_8Cmpd-II(LutD$^+$) obtained at 80 K in the absence of a magnetic field. See Table S10 for the fitted parameters. Both A and B are plausible fits for the data of F_8Cmpd-II(LutD$^+$) due to the similar parameters between F_8Cmpd-II and the hydrogen bonded ferryl derivative, as was previously described.[1] Further, the Mössbauer spectrum of F_8Cmpd-II(LutD$^+$) matched the previously reported Mössbauer spectrum of F_8Cmpd-II(LutH$^+$).[1] (**C**) UV-vis monitoring of the addition of DHA to F_8Cmpd-II(LutD$^+$) at 0.1 mM at -90 °C in 1:9 MeTHF:toluene, resulting in the formation of the ferric aqua species (**blue** to **green**). Inset: Decrease in the absorbance at 546 nm over time. Note: The UV-vis spectrum of F_8Cmpd-II(LutD$^+$) matches F_8Cmpd-II(LutH$^+$) as seen in Figure S4, both have a peak at 546 nm.

Table S11. Mössbauer parameter fits obtained for F_8Cmpd-II(LutD$^+$), two different fits were possible. The complex was made in in 1:9 MeTHF:toluene at 2 mM at -90 ^{o}C and then subsequently frozen. The spectra were recorded at 80 K in the absence of a magnetic field.

	Reduced χ^2	Peak	Relative Area	δ (mm/s)	ΔE_q (mm/s)	Γ (mm/s)
Fit 1	0.647	1	0.606	0.09	2.05	0.21
		2	0.493	0.08	2.29	0.21
Fit 2	1.050	1	1.139	0.09	2.20	0.32

Note:

Reduced χ2: Is the weighted sum of squared-deviations between experimental and fitted data per fitting degree of freedom.

Peak and Reative Area: The number of species and their percentage determined to be in solution.

δ(mm/s): Isomer Shift

ΔEq(mm/s): Quadrupole Spitting

Γ(mm/s): The linewidth of the peaks.

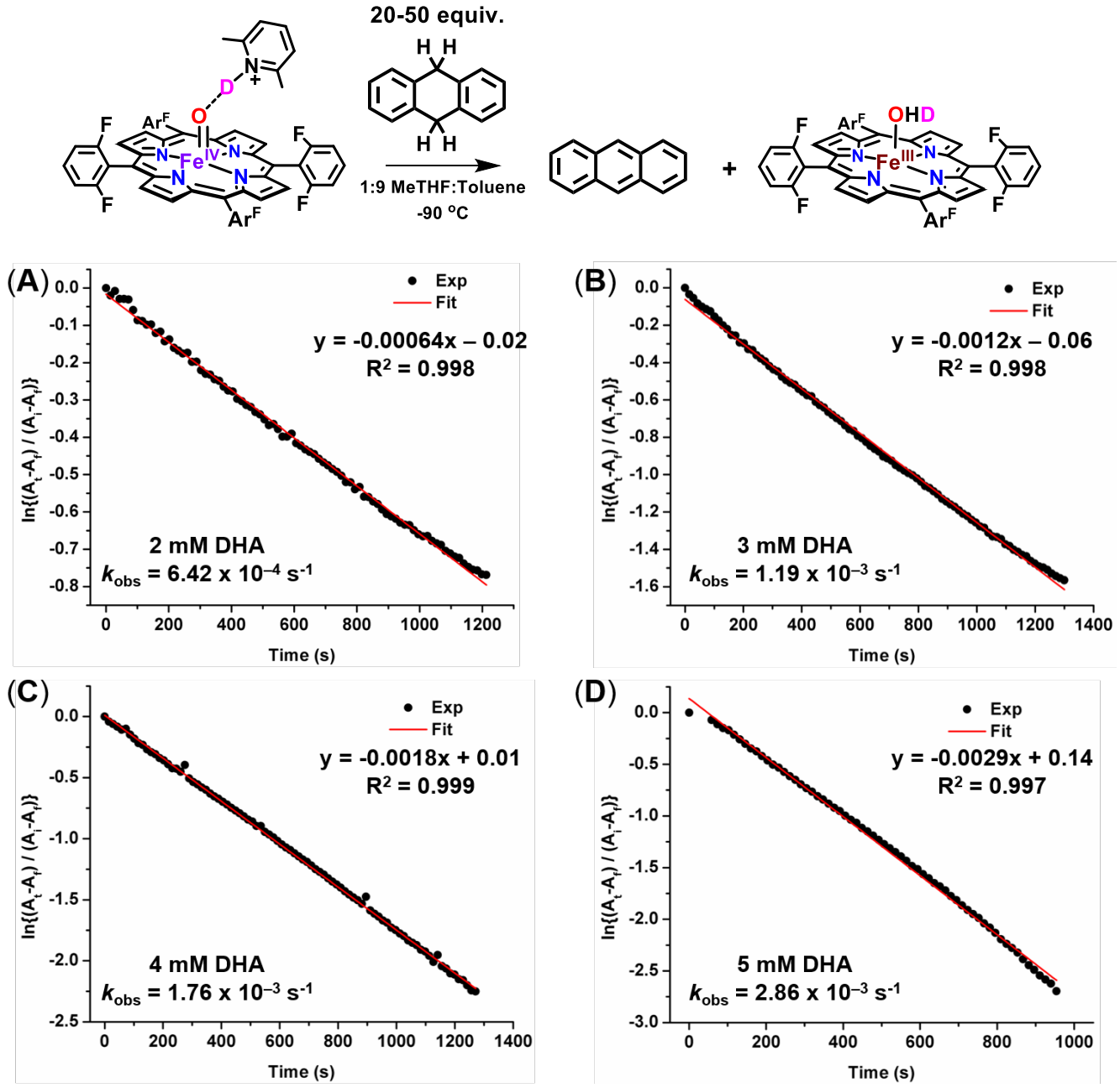

Figure S34. UV-vis spectroscopy monitoring the rate of reaction upon addition of (**A**) 20, (**B**) 30, (**C**) 40, and (**D**) 50 equiv. of 9,10-dihydroanthracene to F_8Cmpd-II(LutD$^+$).

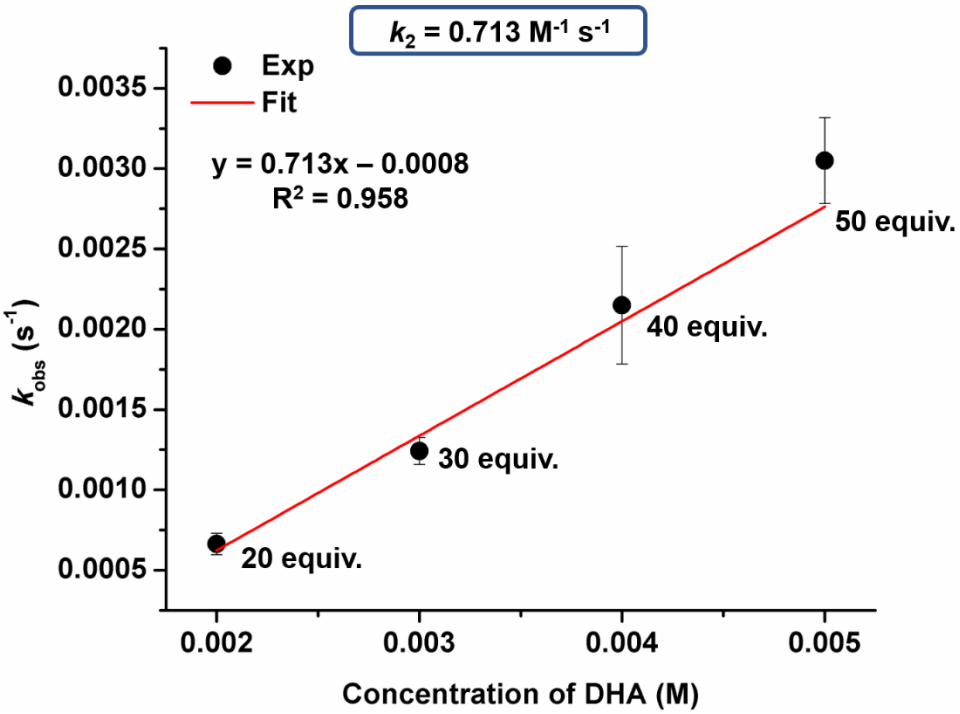

Figure S35. Second order rate constant k_2 determined under pseudo first order conditions of the addition of 9,10-dihydroanthracene to F_8Cmpd-II(LutD$^+$), giving a k_2 = 0.713 ± 0.086 M^{-1} s^{-1}. Each data point is an average of three trials. The error bars are representing the standard deviation.

Table S12. Average and standard deviation for k_{obs} of the reaction between F_8Cmpd-II(LutD$^+$) and DHA. Three trials were run for each concentration of DHA.

Concentration of DHA (M)	Average k_{obs} (s^{-1})	Standard Deviation of k_{obs}
0.002	6.63 x 10^{-4}	6.67 x 10^{-5}
0.003	1.24 x 10^{-3}	8.33 x 10^{-5}
0.004	2.15 x 10^{-3}	3.67 x 10^{-4}
0.005	3.05 x 10^{-3}	2.67 x 10^{-4}

VI. Product Analysis

In order to determine the organic products after the reactions of xanthene with F_8Cmpd-II as well as xanthene and fluorene with F_8Cmpd-II(LutH$^+$), these reactions were run at a higher concentration in order to feasibly quantify the products. Thus, reactions were run at 10 mM Fe concentration in 5 mL Schlenk flasks under air-free conditions at –90 °C. One to five equivalents of substrate were added to either F_8Cmpd-II or F_8Cmpd-II(LutH$^+$) and the resulting reaction mixtures were stirred for 5-10 minutes before 40 μL of a 117 mM solution of dodecane in DCM was added for use as an internal standard (t_R = 5.2 minutes). Then, 2 μL of the reaction mixture were injected into the GC instrument for analysis. Calibration curves of xanthone, fluorenone, and 9,9'-bifluorenyl were obtained in order to quantify the products.

GC method:

Inlet: 320 °C, 8.8 psi, 54.2 mL/min of He flow

Column: 8.8 psi, 1.8 mL/min flow

Oven: Initial oven temperature: 50 °C; Hold Time: 0.4 min

Ramp 1: 25 °C per minute, up to 195 °C; Hold Time: 1.5 min

Ramp 2: 8 °C per min, up to 265 °C; Hold Time: 1.5 min

Ramp 3: 20 °C per min, up to 315 °C; Hold Time: 1.25 min

Detector: Heater: 315 °C; H_2 flow: 30 mL/min; Air flow: 400 mL/min; He flow: 30 mL/min

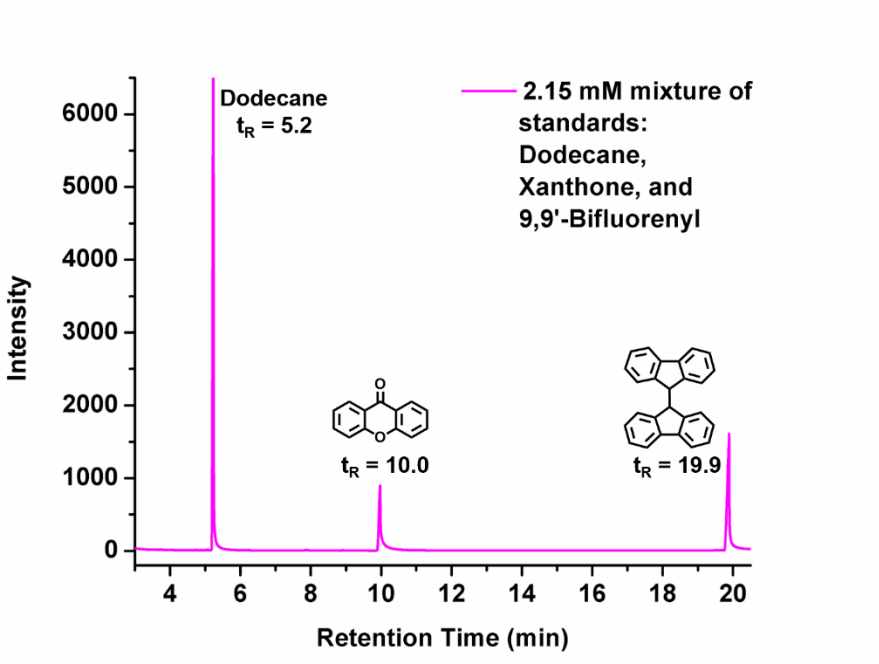

Figure S36. Gas chromatograph of a 2.15 mM solution of dodecane, xanthone, and 9,9'-bifluorenyl in dichloromethane.

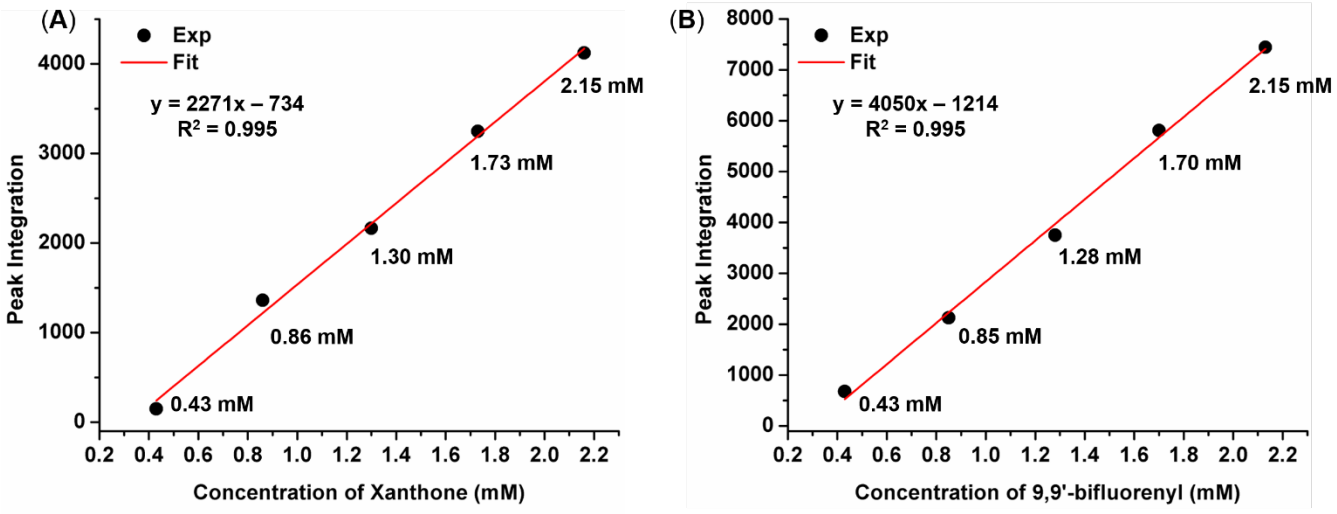

Figure S37. Gas chromatography calibration curves for (**A**) xanthone and (**B**) 9,9'-bifluorenyl.

Table S13. Peak integration (determined from gas chromatography) values for varying concentrations of xanthone and 9,9'-bifluorenyl determined for the calibration curves shown in Figure S37.

Concentration of Xanthone (mM)	Peak Integration	Concentration of 9,9'-bifluorenyl (mM)	Peak Integration
0.43	149	0.43	677
0.86	1361	0.85	2128
1.30	2163.7	1.28	3752
1.73	3248	1.70	5810
2.15	4122	2.15	7442

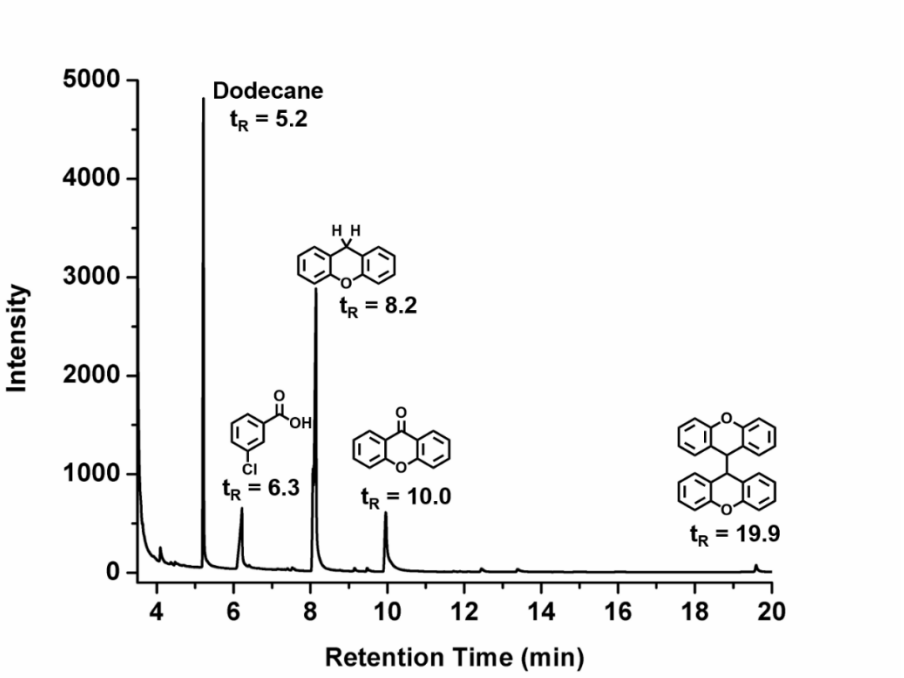

Figure S38. Representative gas chromatograph for an aliquot taken from a reaction mixture of F_8Cmpd-II with xanthene. Compounds identified in the gas chromatograph are shown with their retention times (t_R).

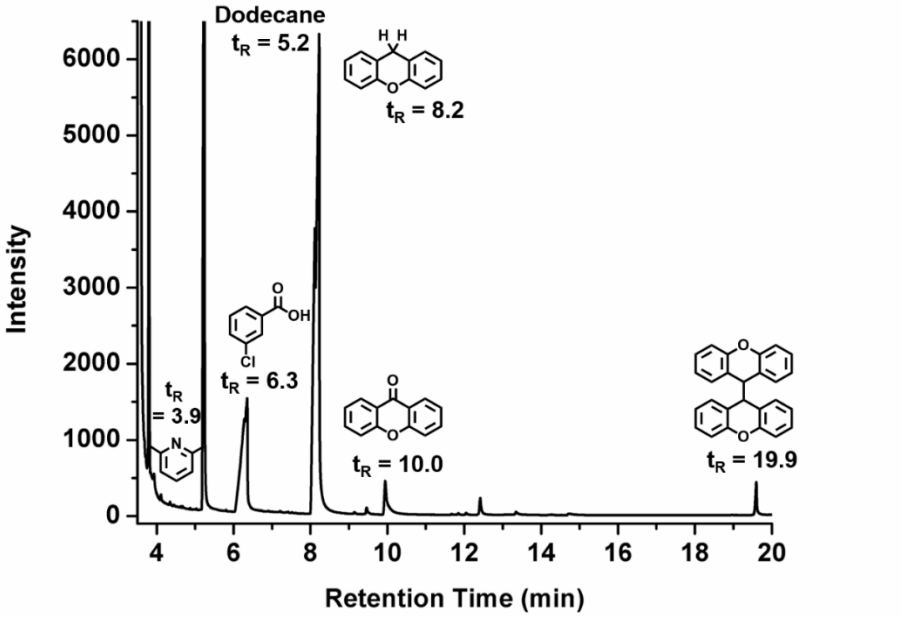

Figure S39. Representative gas chromatograph for an aliquot taken from a reaction mixture of F_8Cmpd-II(LutH$^+$) with xanthene. Compounds identified in the gas chromatograph are shown with their retention times (t_R).

Table S14. Yields obtained for the organic products from reactions of F_8Cmpd-II and F_8Cmpd-II($LutH^+$) with xanthene using the calibration curves in Figure S37. Note, the xanthone yield is based on a 4:1 ferryl:xanthone stoichiometry and the 9,9'-bixanthene yield is based on a 2:1 ferryl:9,9'-bixanthene stoichiometry. See Scheme S2 for a proposed mechanism.

	Xanthone	9,9'-bixanthene	Total % Yield
F_8Cmpd-II	74-85%	13-14%	88-98%
F_8Cmpd-II($LutH^+$)	58-64%	6-12%	70%

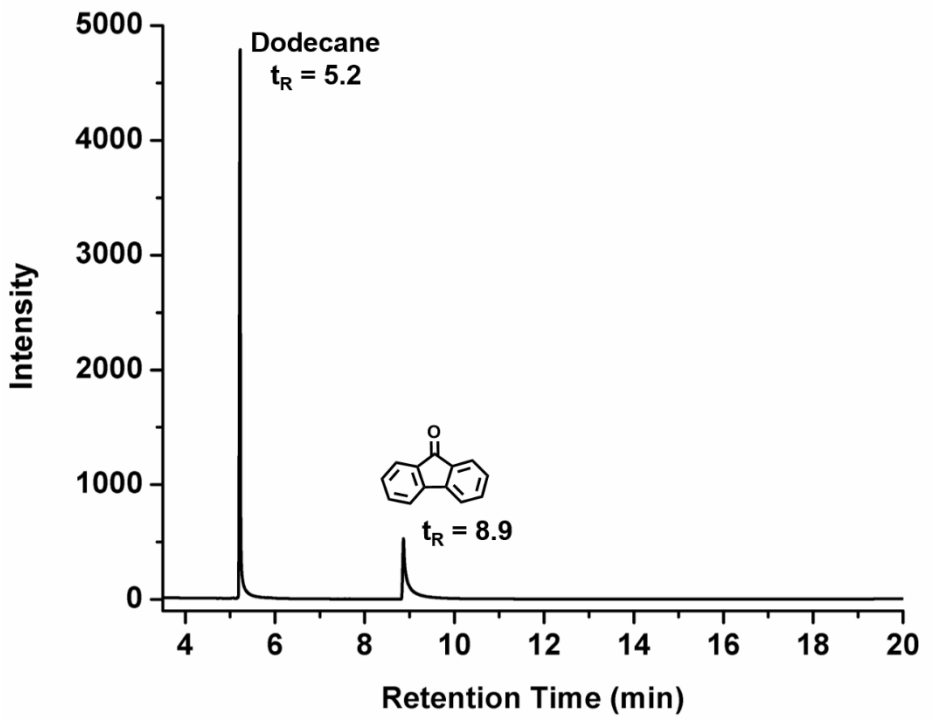

Figure S40. Gas chromatograph of a 2.15 mM solution of dodecane and 2.12 mM fluorenone.

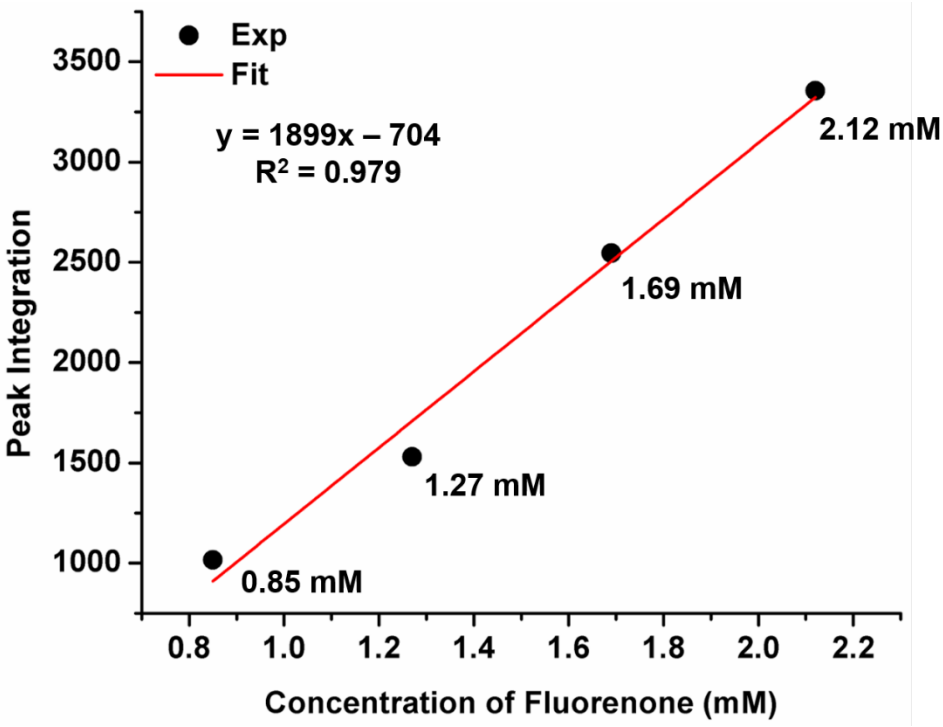

Figure S41. Gas chromatography calibration curve for fluorenone.

Table S15. Peak integration (determined from gas chromatography) values for varying concentrations of fluorenone determined for the calibration curve shown in Figure S41.

Concentration of Fluorenone (mM)	Peak Integration
0.85	1016
1.27	1530
1.69	2546
2.12	3355

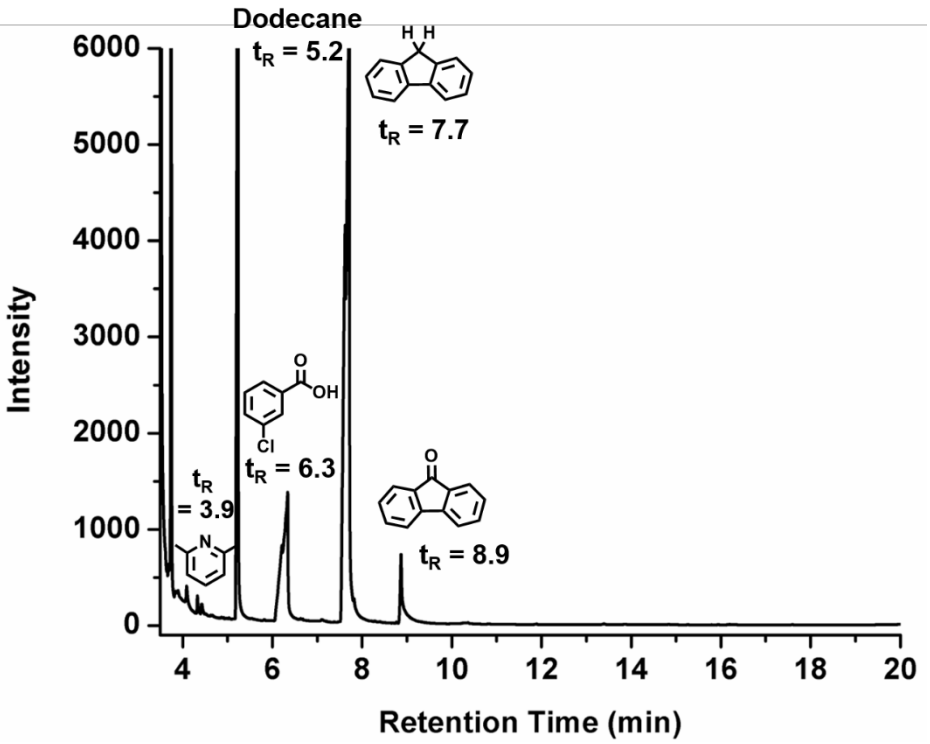

Figure S42. Representative gas chromatograph for an aliquot taken from a reaction mixture of F_8Cmpd-II(LutH$^+$) with fluorene. Compounds identified in the gas chromatograph are shown with their retention times (t_R).

Table S16. Yields obtained for the organic products from reactions of F_8Cmpd-II(LutH$^+$) with fluorene.

	Fluorenone	**9,9'-bifluorenyl**	**Total % Yield**
F_8Cmpd-II(LutH$^+$)	83%	0%	83%

Scheme S1. Reactions of xanthene with F_8Cmpd-II and F_8Cmpd-II(LutH$^+$) result in formation of major product xanthone (**top**) or minor product 9,9'-bixanthene (**bottom**) with the stoichiometries shown.

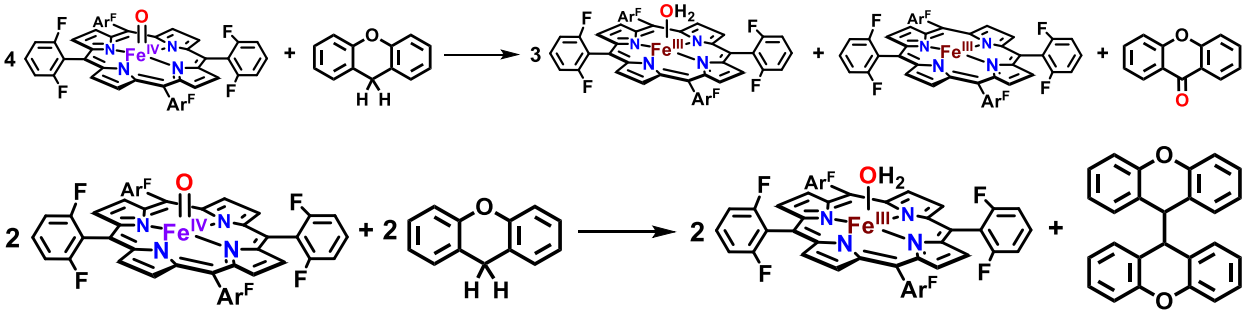

Scheme S2. Proposed mechanism for the formation of xanthone and bisxanthene by F_8Cmpd-II(LutH$^+$). Initial HAA from xanthene (followed by immediate proton transfer) results in formation of $F_8Fe^{III}OH_2$ and xanthenyl radical. Two of these radicals can couple to form bisxanthene. However, the xanthenyl radical may also react with a second equiv. of F_8Cmpd-II(LutH$^+$), undergoing a hydroxylation (rebound) step to form xanthydrol. Xanthydrol can then be easily oxidized by two equiv. of F_8Cmpd-II(LutH$^+$) to give the final xanthone product. A similar mechanism can be proposed for F_8Cmpd-II, with *m*CBA acting as the proton source instead of LutH$^+$ in the steps that require protonation of $F_8Fe^{III}OH$ to give $F_8Fe^{III}OH_2$.

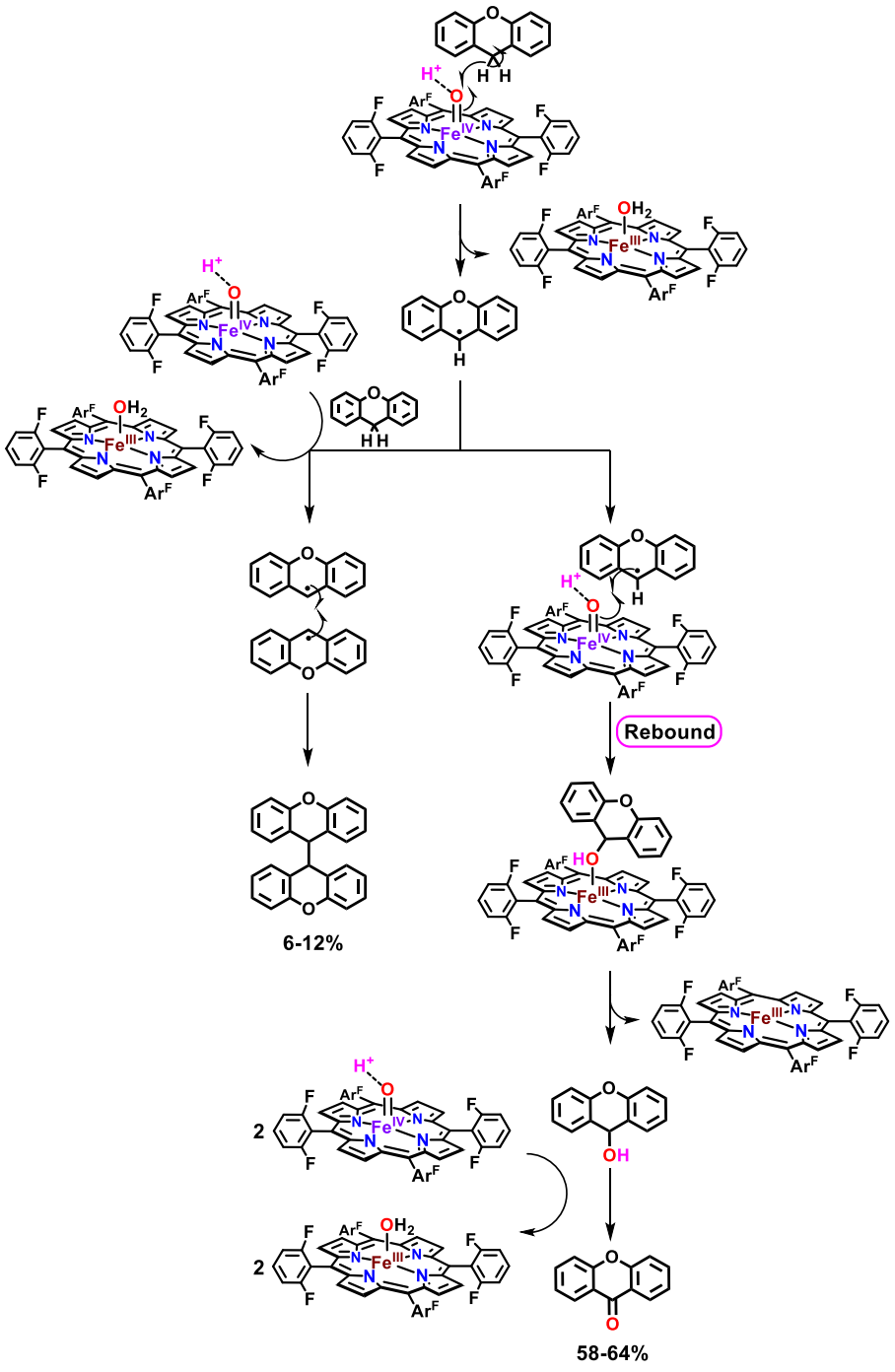

VII. References

(1) Ehudin, M. A. .; Gee, L. B.; Sabuncu, S. ; Braun, A.; Moënne-Loccoz, P.; Hedman, B.; Hodgson, Keith O.; Solomon, E. I.; Karlin, K. D. Tuning the Geometric and Electronic Structure of Synthetic High-Valent Heme Iron(IV)-Oxo Models in the Presence of a Lewis Acid and Various Axial Ligands. *J. Am. Chem. Soc.* **2019**, *141*, 5942–5960.